NAVAL POSTGRADUATE SCHOOL
Monterey, California

THESIS

A SPATIALLY INCOHERENT AND TEMPORALLY COHERENT SOURCE

by

John S. Peterson

June 1984

Thesis Advisor: D. L. Walters

Approved for public release; distribution unlimited

SECURITY CLASSIFICATION OF THIS PAGE (When Data Entered)

REPORT DOCUMENTATION PAGE		READ INSTRUCTIONS BEFORE COMPLETING FORM
1. REPORT NUMBER	2. GOVT ACCESSION NO.	3. RECIPIENT'S CATALOG NUMBER
4. TITLE (and Subtitle) A Spatially Incoherent and Temporally Coherent Source		5. TYPE OF REPORT & PERIOD COVERED Master's Thesis; June 1984 6. PERFORMING ORG. REPORT NUMBER
7. AUTHOR(s) John S. Peterson		8. CONTRACT OR GRANT NUMBER(s)
9. PERFORMING ORGANIZATION NAME AND ADDRESS Naval Postgraduate School Monterey, California 93943		10. PROGRAM ELEMENT, PROJECT, TASK AREA & WORK UNIT NUMBERS
11. CONTROLLING OFFICE NAME AND ADDRESS Naval Postgraduate School Monterey, California 93943		12. REPORT DATE June 1984 13. NUMBER OF PAGES 91
14. MONITORING AGENCY NAME & ADDRESS (if different from Controlling Office)		15. SECURITY CLASS. (of this report) Unclassified 15a. DECLASSIFICATION/ DOWNGRADING SCHEDULE

16. DISTRIBUTION STATEMENT (of this Report)

Approved for public release; distribution unlimited

17. DISTRIBUTION STATEMENT (of the abstract entered in Block 20, if different from Report)

18. SUPPLEMENTARY NOTES

19. KEY WORDS (Continue on reverse side if necessary and identify by block number)

Spatially Incoherent Light Source
Young's Double Slit Experiment

20. ABSTRACT (Continue on reverse side if necessary and identify by block number)

The ability to create a spatially incoherent and temporally coherent source is a major military concern when considering atmospheric turbulence effects on laser beam propagation. Young's double slit experiment is used to measure the degree of spatial coherence of the source when various diffusive materials are placed between the laser and double slit. A photo-multiplier tube is used for detection of an argon-ion

DD FORM 1 JAN 73 1473 EDITION OF 1 NOV 65 IS OBSOLETE

S N 0102-LF-014-6601

SECURITY CLASSIFICATION OF THIS PAGE (When Data Entered)

20. (Continued)

laser signal. Experimental results show that the spatial coherence of the source is affected significantly by the location of the diffusive material and the size of the laser beam. For this particular experimental geometry, opal glass placed 17 cm from the double slit degrades the spatial coherence of the source by 99.5%. By expanding the beam diameter 2 1/2 times the original size, the spatial coherence of a diffused beam is decreased by an average of 95% over a 10 cm region. In addition to experimental observations, the applicable sections of partial coherence theory are discussed.

Approved for public release; distribution unlimited

A Spatially Incoherent and Temporally Coherent Source

by

John S. Peterson
Lieutenant, United States Navy
B.S., United States Naval Academy, 1978

Submitted in partial fulfillment of the
requirements for the degree of

MASTER OF SCIENCE IN PHYSICS

from the

NAVAL POSTGRADUATE SCHOOL
June 1984

ABSTRACT

The ability to create a spatially incoherent and temporally coherent source is a major military concern when considering atmospheric turbulence effects on laser beam propagation. Young's double slit experiment is used to measure the degree of spatial coherence of the source when various diffusive materials are placed between the laser and double slit. A photo-multiplier tube is used for detection of an argon-ion laser signal. Experimental results show that the spatial coherence of the source is affected significantly by the location of the diffusive material and the size of the laser beam. For this particular experimental geometry, opal glass placed 17 cm from the double slit degrades the spatial coherence of the source by 99.5%. By expanding the beam diameter 2 1/2 times the original size, the spatial coherence of a diffused beam is decreased by an average of 95% over a 10 cm region. In addition to experimental observations, the applicable sections of partial coherence theory are discussed.

TABLE OF CONTENTS

I. INTRODUCTION 10

II. THEORETICAL CONSIDERATIONS 12

A. SPATIAL COHERENCE 12

B. TEMPORAL COHERENCE 12

C. COHERENCE TIME AND COHERENCE LENGTH 12

D. COMPLEX ANALYTIC SIGNAL 14

E. MUTUAL COHERENCE FUNCTION 15

F. COMPLEX DEGREE OF COHERENCE 16

III. MEASUREMENT OF SPATIAL COHERENCE 19

A. YOUNG'S INFERFEROMETER 19

B. FRINGE VISIBILITY 21

C. RELATIONSHIP BETWEEN F.V. AND $|\gamma_{12}(\tau)|$ 22

D. THE VAN CITTERT-ZERNIKE THEOREM 23

IV. EXPERIMENTAL CONDITIONS 26

A. EQUIPMENT DESCRIPTION 26

B. EXPERIMENT #1 32

C. EXPERIMENT #2 53

D. EXPERIMENT #3 62

E. ERROR ANALYSIS 73

1. Alignment 73

2. Effect of Finite Slit Width of the Photomultiplier Aperture 74

3. Scattered Light 79

4. Fringe Visibility Measurements 82

5. Double Slit Measurements 83

V. CONCLUSION 86

APPENDIX A: PROOF THAT F.V. = $|\gamma_{12}(\tau)|$ 87

LIST OF REFERENCES 90

INITIAL DISTRIBUTION LIST 91

LIST OF FIGURES

1. Young's Double Slit Experiment 20

2. Schematic Diagram for Detection Apparatus 27

3. Micro-Ammeter and Power Supplies for Detector . . . 28

4. X-Y Recorder 29

5. Photomultiplier Mounted on Micrometer Slide 30

6. Argon Ion Laser 31

7. Quantum Efficiency for RCA 1P21 Photomultiplier 33

8. Intensity Measurement Using He-Ne Laser (4% Milk/Water Diffuser) 34

9. Ground Glass, Ground Glass/Opal Glass, and Opal Glass 35

10. Diagram for Experiment #1 36

11. Interference Pattern for Ground Glass 10 cm from Slits 39

12. Interference Pattern for Ground Glass 30 cm from Slits 40

13. Interference Pattern for Ground Glass 60 cm from Slits 41

14. Interference Pattern for Opal/Ground Glass 20 cm from Slits 42

15. Interference Pattern for Opal Glass 15 cm from Slits 43

16. Interference Pattern for Opal Glass 17 cm from Slits 44

17. Interference Pattern for Opal Glass 18 cm from Slits 45

18. Interference Pattern for Opal Glass 40 cm from Slits 46

19. Plot of Coherence vs Distance for Ground Glass . . . 48

20. Plot of Coherence vs Distance for Opal/Ground Glass 50

21. Plot of Coherence vs Distance for Opal Glass 52

22. Interference Pattern with Collimating Lens Between Opal and Double Slit 54

23. Interference Pattern for Single Slit 30 cm from Double Slit 55

24. Plot of Coherence vs Distance for Single Slit . . . 56

25. Interference Pattern for Pinhole 10 cm from Double Slit 58

26. Interference Pattern for Pinhole 25 cm from Double Slit 59

27. Plot of Coherence vs Distance for Pinhole 61

28. Gaussian Profile for Raw laser Beam (1.5 mm) 63

29. Gaussian Profile for 2.9 mm Diameter Beam 64

30. Interference Pattern for Opal at 17 cm (2.9 mm Beam) 65

31. Interference Pattern for Opal at 30 cm (2.9 mm Beam) 66

32. Interference Pattern for Opal at 21 cm (3.6 mm Beam) 67

33. Interference Pattern for Opal at 40 cm (3.6 mm Beam) 68

34. Plot of Coherence vs Distance for Opal (2.9 mm Beam) 70

35. Plot of Coherence vs Distance for Opal (3.6 mm Beam) 72

36. Interference Pattern Using Pinhole Aperture on PM Tube 75

37. Interference Pattern Using Narrow Slit Aperture on PM Tube 76

38. Interference Pattern Using Wide Slit Aperture on PM Tube 77

39. Plot Showing Effect of Finite Slit Width and Scattering on Coherence Measurements 80

40. Interference Pattern with Baseline Corrected for Finite Slit Width and Scattering 81

41. Single Slit Diffraction Patterns for Beams with Different Diameters 85

I. INTRODUCTION

The purpose of this experimental research is to determine if it is possible to destroy the high degree of spatial coherence of a laser source and yet maintain the temporal coherence of the field. The concept of partial coherence has become important in almost every branch of physics. At the Naval Postgraduate School, the motivation for creating an incoherent source is in connection with atmospheric effects on laser propagation.

For simplicity, coherence theory is usually discussed in terms of complete coherence or complete incoherence. However, each of these limiting extremes describe artificial concepts which are only mathematical idealizations. This thesis deals with partial coherence, the intermediate state between complete coherence and complete incoherence.

Because the theory of partial coherence involves statistical aspects of electromagnetic theory, functions used in the study of partial coherence deal with average values of parameters describing the electromagnetic field. The correlation functions that are applicable to spatial coherence are described as well as the fundamental concepts of coherence.

The classical method of Young's double slit experiment was used to measure the spatial coherence of the source. Several diffusive materials were placed between the laser and the double slits in an attempt to degrade the spatial coherence of the laser. The experimental observations and results are discussed.

II. THEORETICAL CONSIDERATIONS

A. SPATIAL COHERENCE

The concept of spatial coherence can be most clearly understood by considering two points of an electromagnetic (e.m.) wave. If two points, $P(r_1,t)$ and $P(r_2,t)$, lie on the same wavefront of a given e.m. wave, then the difference between the phases of the electric fields at the two points is zero at time $t = 0$. If the phase difference remains zero for $t > 0$, then the two points are perfectly coherent. If this occurs for any two points on the wavefront then the wave has perfect spatial coherence.

B. TEMPORAL COHERENCE

Temporal coherence of an e.m. field exists if the phase difference between two points in the field, $P(r_1,t_1)$ and $P(r_1,t_2)$, remains constant for different times, t_1 and t_2. If this happens for any time interval, then the wave has perfect temporal coherence.

C. COHERENCE TIME AND COHERENCE LENGTH

Another interpretation of temporal coherence involves the coherence time, Δt, which is the reciprocal of the frequency bandwidth. If the light source is perfectly monochromatic, the bandwidth is zero and the coherence time

is infinite. This is an idealization that cannot occur in practice. However, a wave behaves as if it is monochromatic, or quasi-monochromatic, if the relevant time interval for a particular situation is much shorter than the coherence time. The coherence time can be thought of as the time interval over which the phase of the wave can be predicted. If the coherence time is large, the wave has a high degree of temporal coherence.

The longitudinal spatial coherence can be interpreted in terms of the coherence length, $c\Delta t$. If the coherence length is much larger than the distance between two points lying on a radius from a quasi-monochromatic light source, then a single wave train can extend over the entire separation. The disturbances at each point are highly correlated. However, if the separation between the two points is much larger than the coherence length, then many wave trains with different phases will lie between these points. In this case, the disturbances at the two points are totally independent of each other and they are considered to be longitudinally incoherent.

The amount of lateral spatial coherence can be determined by measuring the superposition of the e.m. fields of two laterally spaced points in the distant radiation field. If a quasi-monochromatic source illuminates two apertures on an opaque surface, the apertures serve as a

source of secondary Huygen wavelets which will generate an interference pattern in the Fraunhofer region. The spatial coherence is proportional to the modulation of this interference pattern.

D. COMPLEX ANALYTIC SIGNAL

Svelto [Ref. 1] introduces the Complex Analytic Signal by starting with a complex representation of a polychromatic light field. This approach treats the e.m. wave as a scalar field with linear polarization. Using a Fourier expansion the real field variable is

$$V^r(\vec{r},t) = \frac{1}{2\pi} \int_{-\infty}^{\infty} V(\vec{r},w)\ \exp(-iwt)\,dw\ . \qquad (1)$$

The inverse relationship for equation (1) is,

$$V(\vec{r},w) = \int_{-\infty}^{\infty} V^r(\vec{r},t)\ \exp(iwt)\,dt\ . \qquad (2)$$

Since V^r is real, $V(\vec{r},-w) = V^*(\vec{r},w)$[1], which suggests that only the positive frequency spectrum is required since the negative frequencies do not add additional information. Therefore, the complex analytic signal is defined by,

---

[1]The asterisk symbol represents complex conjugate.

$$V(\vec{r},t) = \frac{1}{\pi} \int_0^\infty V(\vec{r},w) \exp(-iwt)dw \quad . \tag{3}$$

The intensity of the beam in terms of the analytic signal is,

$$I(\vec{r},t) = \langle V(\vec{r},t)\ V^*(\vec{r},t)\rangle \quad , \tag{4}$$

where the brackets indicate a time average over a time interval that is long compared to the coherence time.

E. MUTUAL COHERENCE FUNCTION

The function used for the analysis of the most basic coherence effects in optics is the "mutual coherence function." Wolf [Ref. 2] defines the mutual coherence function as,

$$\Gamma_{12}(\tau) = \langle V_1(t+\tau)\ V_2^*(t)\rangle \quad , \tag{5}$$

where $V_1(t)$ and $V_2(t)$ are the complex field disturbances at two different points and τ is a time delay. Other notations include $\Gamma_{12}(\tau) = \Gamma(\vec{r}_1,\vec{r}_2,\tau)$ and $V_1(t+\tau) = V(\vec{r}_1,t+\tau)$ to explicitly emphasize the spatial dependence of the variables.

F. COMPLEX DEGREE OF COHERENCE

The normalized form of the mutual coherence function is known as the "complex degree of coherence" and is defined as,

$$\gamma_{12}(\tau) = \frac{\Gamma_{12}(\tau)}{[\Gamma_{11}(0)\Gamma_{22}(0)]^{1/2}} = \frac{\Gamma_{12}(\tau)}{[I_1 I_2]^{1/2}} \quad , \qquad (6)$$

where from eqn. 4 and eqn. 5,

$$I_j = \Gamma_{jj}(0) = \langle V_j(t) V_j^*(t) \rangle \quad , \ (j=1,2) \quad . \qquad (7)$$

From eqn. 7 and the Cauchy-Schwartz inequality the values of the modulus of $\gamma_{12}(\tau)$ lie between 0 and 1. The disturbances at $\vec{r}_1$ and $\vec{r}_2$ are considered to be coherent if $|\gamma_{12}(\tau)| = 1$, and they are incoherent if $|\gamma_{12}(\tau)| = 0$. When $0 < |\gamma_{12}(\tau)| < 1$, partial coherence exists. A summary of the values for $|\gamma_{12}(\tau)|$, which is known as the "degree of coherence", is listed in Table 1.

In addition, a first-order correlation function between two different points, r_1 and r_2 at the same instant of time can be defined as,

$$\Gamma_{12}(0) = \langle V_1(t)\ V_2^*(t) \rangle \quad . \qquad (8)$$

The corresponding normalized function $\gamma_{12}(0)$ is defined as,

TABLE I

SUMMARY OF DEGREE OF COHERENCE

$\lvert\gamma_{12}(\tau)\rvert = 0$	Incoherent Limit
$0 < \lvert\gamma_{12}(\tau)\rvert < 1$	Partial Coherence
$\lvert\gamma_{12}(\tau)\rvert = 1$	Coherent Limit

$$\gamma_{12}(0) = \frac{\Gamma_{12}(0)}{[\Gamma_{11}(0)\Gamma_{22}(0)]^{1/2}} , \qquad (9)$$

where $\Gamma_{11}(0) = \Gamma(\vec{r}_1,\vec{r}_1,0)$. The quantity $\gamma_{12}(0)$ is called the "complex degree of spatial coherence." For partially coherent light, $\gamma_{12}(0)$ decreases from the value 1 (where $r_2 = r_1$) to zero as $|r_2 - r_1|$ increases. One of the primary goals of this thesis is to measure the degree of spatial coherence, $|\gamma_{12}(0)|$, under various experimental conditions.

III. MEASUREMENT OF SPATIAL COHERENCE

A. YOUNG'S INTERFEROMETER

One method used to measure the degree of spatial coherence, $|\gamma_{12}(0)|$, between two points of a light wave is through the use of Young's double slit interferometer. In addition to demonstrating the measurability of $|\gamma_{12}(0)|$ this experiment illustrates its significance. Figure 1 shows a simplified experimental set-up consisting of a quasi-monochromatic source illuminating two parallel, narrow, closely spaced slits S_1 and S_2. When symmetry exists, the segments of the primary wavefront arriving at the two slits will be exactly in phase, and the slits will constitute two coherent secondary line sources. If the optical path difference[2] is less than the coherence length, the waves emitted from the slits will interfere and form a fringe pattern in the plane of observation. The interference at point P and at time t will result from the waves emitted from the slits from points S_1 and S_2 at times $t - \frac{L_1}{c}$ and $t - \frac{L_2}{c}$. The interference fringes become more distinct as the correlation between the two analytic signals increases. The analytic signals are $V[S_1, t - \frac{L_1}{c}]$ and $V[S_2, t - \frac{L_2}{c}]$.

---

[2] $OPD = S_2B = n(L_2 - L_1)$ where n is the index of refraction ($n_{air} = 1$).

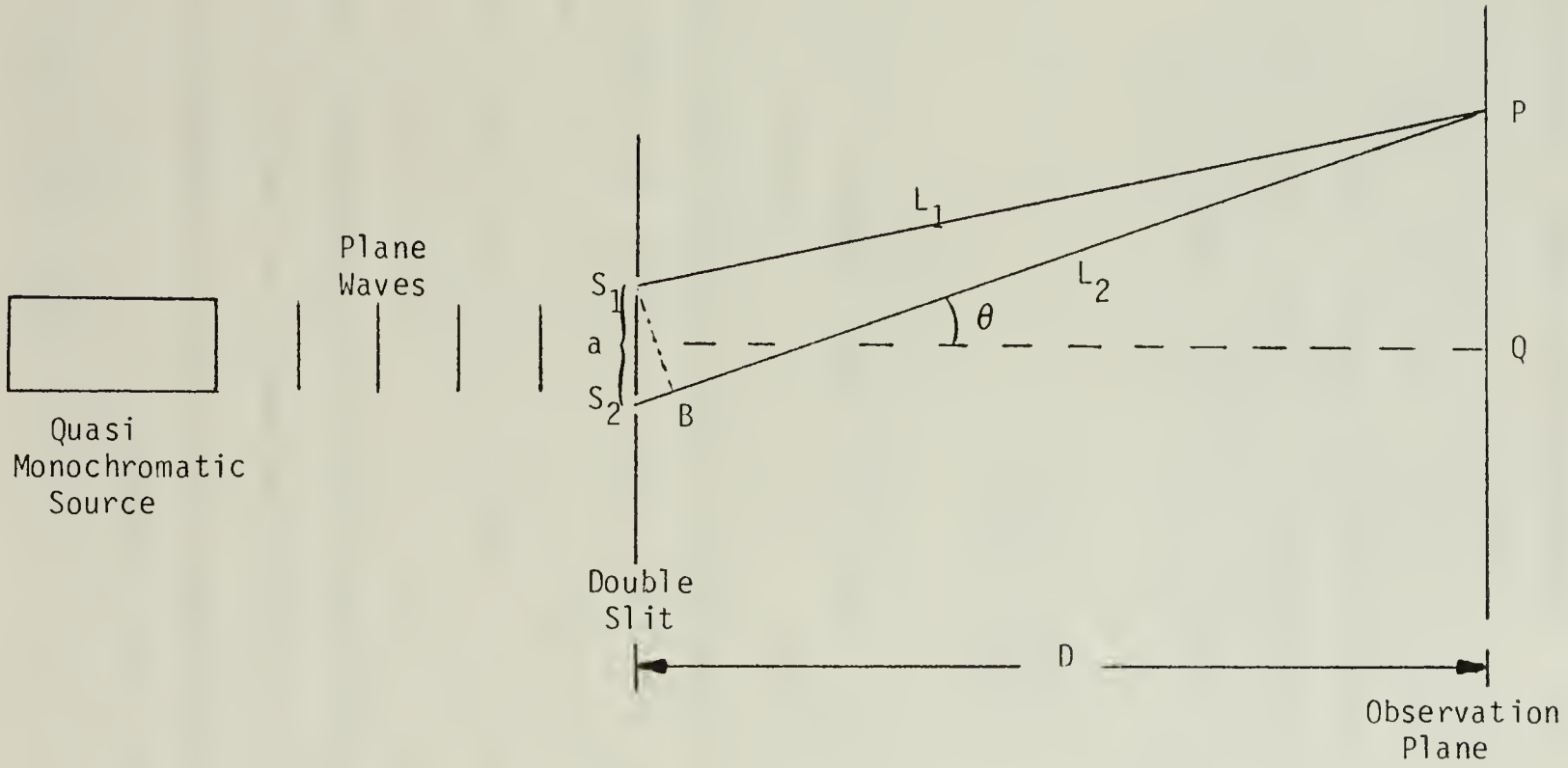

Figure 1. Young's Double Slit Experiment

B. FRINGE VISIBILITY

If point Q is chosen in the observation plane of Fig. 1 such that $L_1 = L_2$, the visibility of the fringes around Q will give a measure of the degree of spatial coherence between points S_1 and S_2 for a zero time delay. The Fringe Visibility, as formulated by Michelson [Ref. 3], describes the quality of the fringes produced by the interferometer. The Fringe Visibility[3] at point Q is defined as,

$$F.V. = \frac{I_{max} - I_{min}}{I_{max} + I_{min}} , \qquad (10)$$

where I_{max} and I_{min} are the maximum intensity of a bright fringe and the minimum intensity of an adjacent dark fringe, respectively, in the region of Q. If the two slits produce the same illumination at point Q and if the wave has perfect spatial coherence, then $I_{min} = 0$ and F.V. = 1. For the case in which the analytic signals at S_1 and S_2 are completely incoherent, $I_{max} = I_{min}$, F.V. = 0, and the fringes disappear. For partially coherent illumination the visibility of the fringes decreases as the point of observation is moved away from the central maximum of the pattern. If the path difference, $L_2 - L_1$, is increased beyond a certain limit, the visibility diminishes

---

[3]The notation for visibility is often denoted by script V.

completely. These observations make it clear that it is not adequate to state simply that coherent light interferes and incoherent light does not interfere.

C. RELATIONSHIP BETWEEN F.V. AND $|\gamma_{12}(\tau)|$

The visibility of the fringes, F.V., and the degree of spatial coherence, $|\gamma_{12}(\tau)|$, are related mathematically. If both slits produce different illumination at point P, $I_1 \neq I$. The visibility of the fringes at point P is given by

$$\text{F.V.} = \frac{2(I_1 I_2)^{1/2}}{I_1 + I_2} |\gamma_{12}(\tau)| \quad . \tag{11}$$

If the two slits produce equal illumination at point P, $I_1 = I_2$, and,

$$\text{F.V.} = |\gamma_{12}(\tau)| \quad . \tag{12}$$

Therefore, by measuring the amount of interference as determined by the fringe visibility at a point such that $L_1 = L_2$, the degree of spatial coherence, $|\gamma_{12}(0)|$, between two points, S_1 and S_2, can be obtained. A proof of eqn. 12 is contained in Appendix A.

D. THE VAN CITTERT-ZERNIKE THEOREM

In 1936 van Cittert showed that the optical disturbance is normally distributed in a plane that is illuminated by an incoherent, nearly monochromatic source. One of the theorems in his paper [Ref. 4] shows the relationship between the correlation in the illuminated plane with the intensity distribution across the source plane. Van Cittert calculated exact partition functions which show the correlation between amplitudes in different points without introducing a degree of coherence. This method becomes difficult when dealing with general optics problems.

F. Zernike [Ref. 5] resolved this difficulty by starting with a fundamentally different definition of incoherence. He stated that "Two vibrations of light shall be called incoherent if their superposition gives no visible interferences." Zernike used Young's experiment to show that the interference fringes gradually disappear as the separation between the pinholes becomes greater. The fringes disappear completely with a broad source. For intermediate sizes of the source the fringes do not disappear, but they are less visible than with a point source. In this same paper Zernike stated that "the degree of coherence of two light vibrations shall be equal to the visibility of the interference fringes that may be obtained from them under the best circumstances." The "best

circumstances" suggests that the pinholes are equally illuminated and only small path differences are introduced. The usefulness of Zernike's concept is that the degree of coherence can be calculated directly from the illumination data.

The mathematical formulation of these concepts, known as the van Cittert-Zernike Theorem, can be easily summarized. Zernike [Ref. 6] introduced the "mutual intensity", J_{12}, and defined it as,

$$J_{12} = \int_{\sigma} I(S) \frac{e^{ik(R_1-R_2)}}{R_1 R_2} dS \quad , \tag{13}$$

where k is the wave number and R_1 and R_2 denote the distances between a point, S, on the source, σ, and two points in the observation plane. The "complex coherence factor", μ_{12}, is,

$$\mu_{12} = \frac{1}{[I_1 I_2]^{1/2}} \int_{\sigma} I(S) \frac{e^{ik(R_1-R_2)}}{R_1 R_2} dS \quad , \tag{14}$$

where

$$I_1 = J_{11} = \int_{\sigma} \frac{I(S)}{R_1^2} dS$$

and

$$I_2 = J_{22} = \int_{\sigma} \frac{I(S)}{R_2^2}\, dS$$

are the intensities at P_1 and P_2.

If the time delay is small, such that $\tau << 1/\Delta\nu$, then the mutual intensity and the spatial mutual coherence function can be considered equal. The mutual intensity becomes,

$$J_{12} = \Gamma_{12}(0) = \langle V_1(t) V_2^*(t) \rangle \quad .$$

Similarly, the complex coherence factor becomes,

$$\mu_{12} = \gamma_{12}(0) = \frac{J_{12}}{[I_1\ I_2]^{1/2}} \quad . \tag{15}$$

Therefore, the correlation between the vibrations at any two points P_1 and P_2 in the field can be described by the mutual intensity, J_{12}, and the complex coherence factor, μ_{12}--quantities which depend on the positions of the two points and not on the time difference.

IV. EXPERIMENTAL CONDITIONS

A. EQUIPMENT DESCRIPTION

Figure 2 is a schematic diagram of the apparatus used to measure and record the intensity distribution of the far field interference pattern of Young's double slit experiment. An HP 425A micro-ammeter (Figure 3) was set at 3 nanoamps for all readings and the photomultiplier voltage was adjusted between 0-500 volts on the HP 6515A DC power supply to scale the intensity properly on the X-Y Recorder (Figure 4). An RCA 1P21 photo-multiplier tube was mounted on a micrometer slide (Figure 5) which, when rotated by hand, moved the photo-multiplier across the observation plane. A 5 cm scan of the photomultiplier on the micrometer slide corresponded to 21.9 cm on the abscissa of the X-Y recorder. A narrow slit (.24 mm wide) aperture was used on the photo-multiplier to get an average value of the light field. A blue filter (.488 μm) was mounted over the slit on the photomultiplier tube to remove noise from extraneous light sources.

A Spectra-Physics Argon-Ion laser, model 262, (TEM_{oo}, λ = .488 μm) was used as the light source (Figure 6) to optimize the detection of the interference pattern. The photo-multiplier tube (S-4 spectral response) has a higher

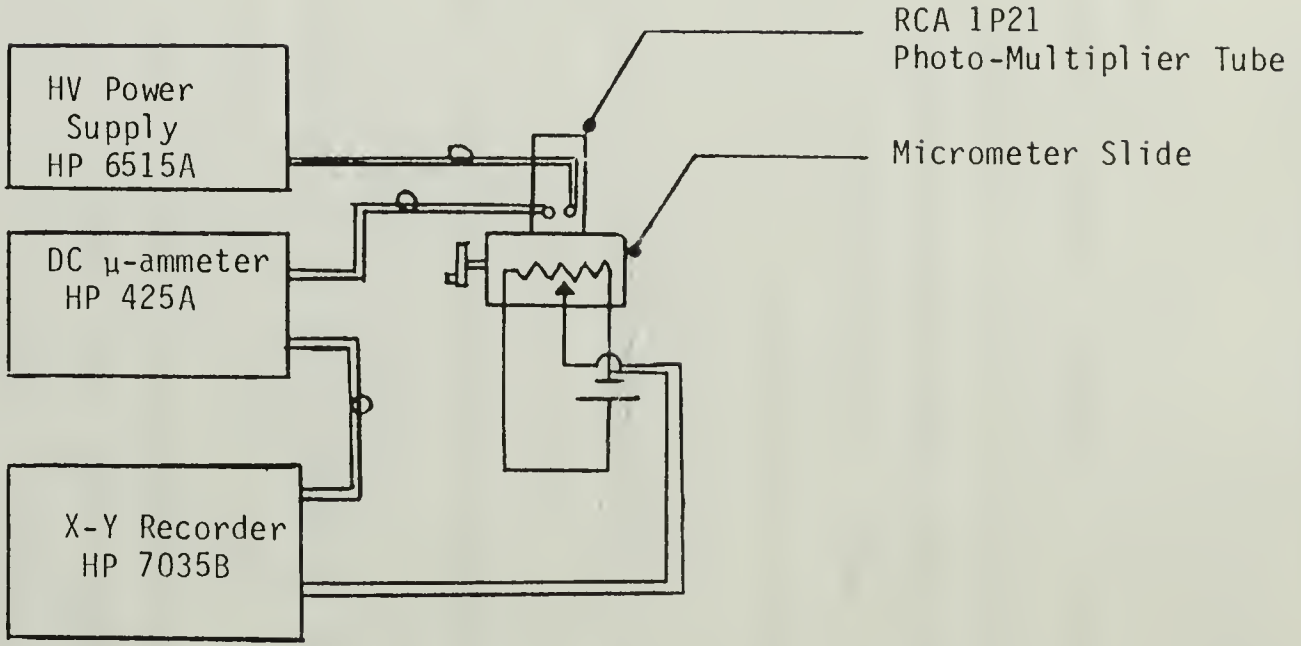

Figure 2. Schematic Diagram for Detection Apparatus

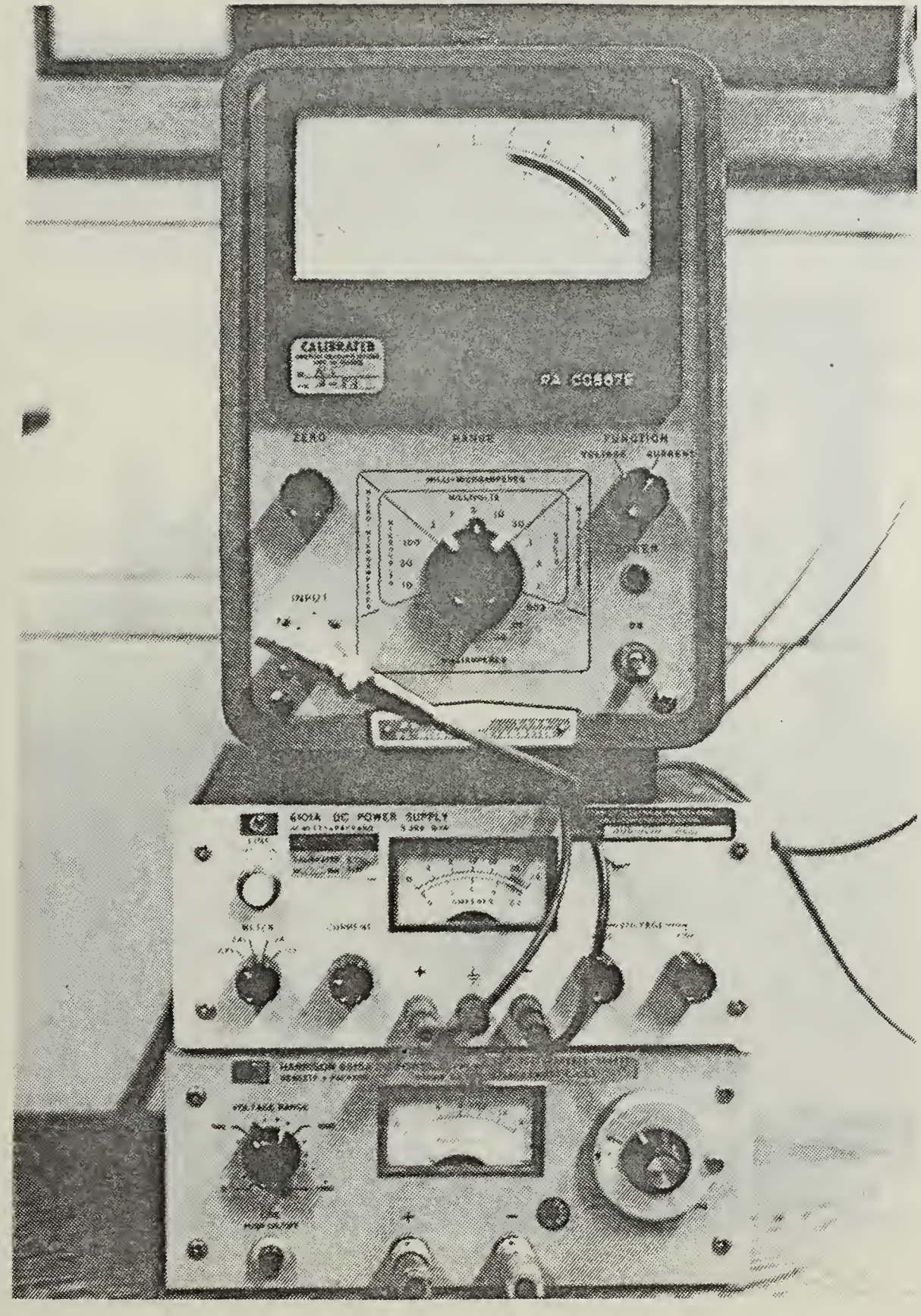

Figure 3. Micro-Ammeter and Power Supplies for Detector

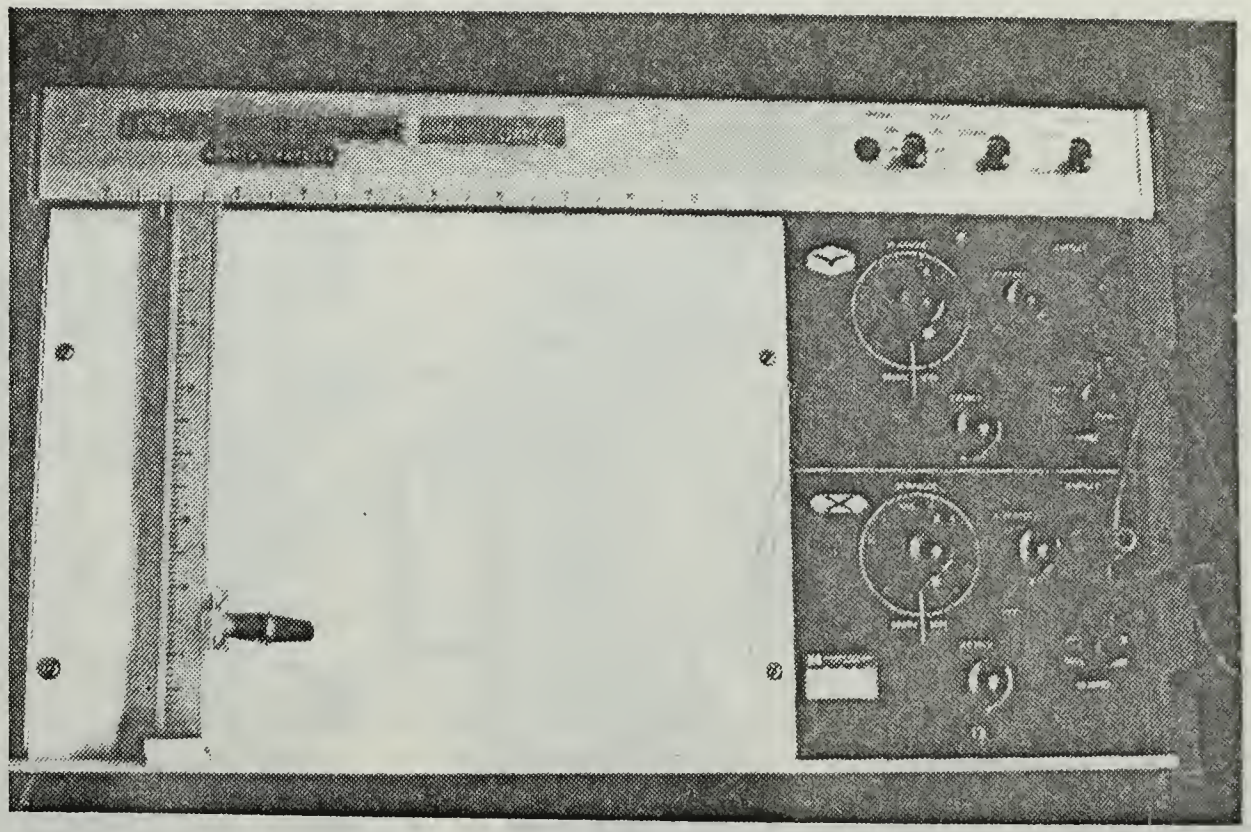

Figure 4. X-Y Recorder

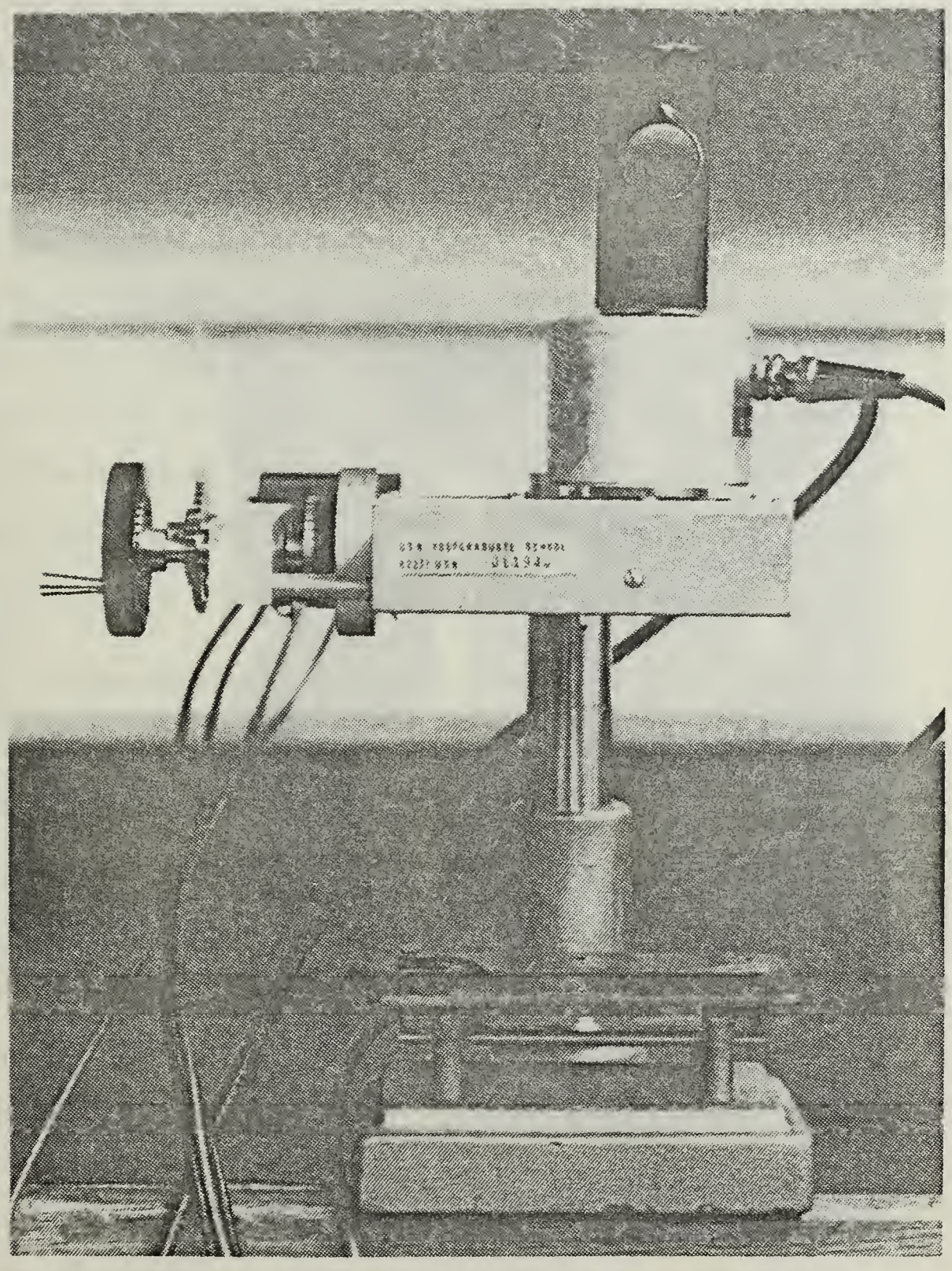

Figure 5. Photomultiplier Mounted on Micrometer Slide

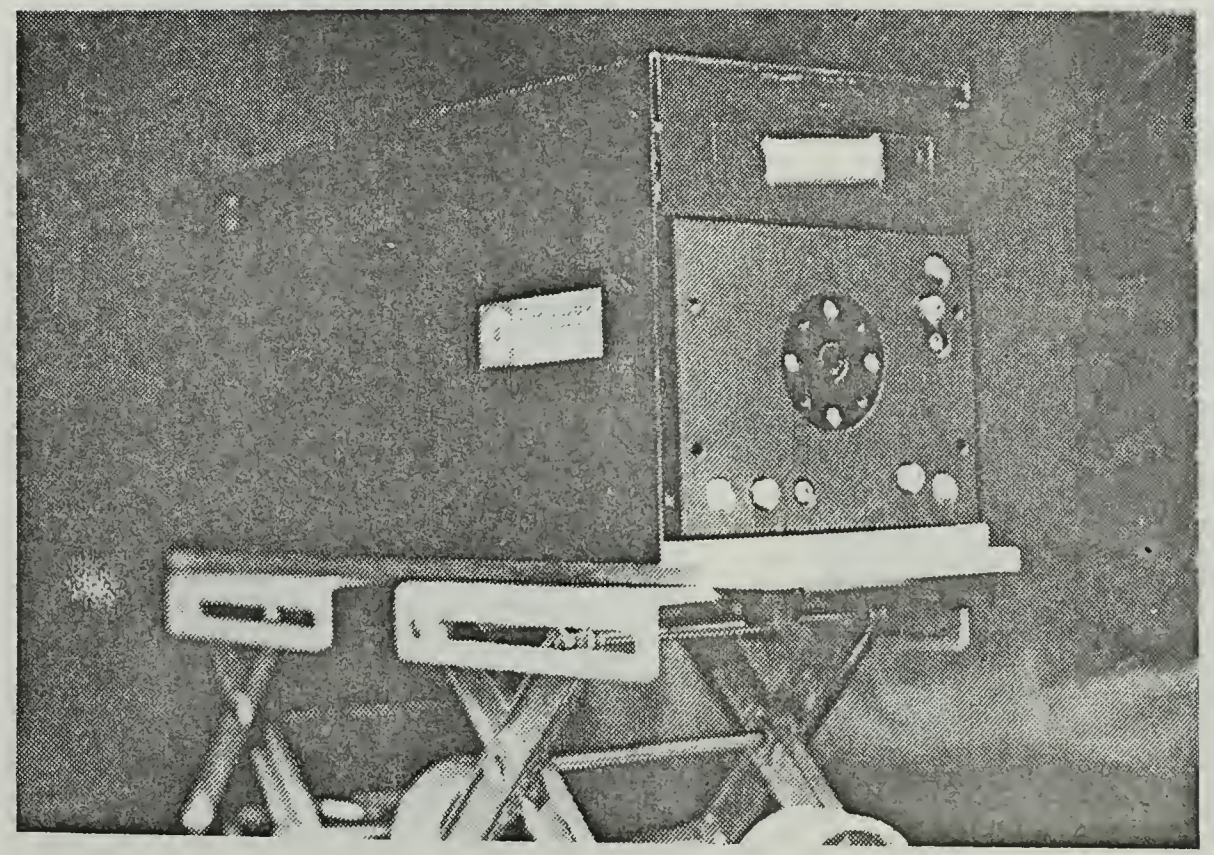

Figure 6. Argon Ion Laser

quantum efficiency, 7%, for blue light and is therefore better suited for the argon-ion laser. Initially, a helium-neon laser was used. When the beam of the He-Ne laser (λ = .633 μm) was attenuated by a diffusive medium, the noise became significant due to the low quantum efficiency, .4%, of the S-4 tube for red light. Figure 7 shows the quantum efficiency as a function of wavelength. Figure 8 shows the intensity measurement for a 4% milk/water solution placed between the He-Ne laser and double slit. Clearly, the noise masks the interference pattern when using the He-Ne laser with the RCA 1P21 photomultiplier.

B. EXPERIMENT #1

Young's double slit experiment was used to measure the degree of spatial coherence of the light field with a diffusive medium inserted between the laser and the double slits. Ground glass, a combination of ground glass and opal glass, and opal glass were used (Figure 9). Figure 10 shows a diagram of this experimental set-up.

Inserting the diffusive medium into the laser beam caused a high degree of scattered light. In order to prevent the scattered light from reaching the detector it was necessary to make an enclosure for the double slits and diffusive medium. This was done by using two boards drilled with apertures and attaching a black cloth cover to the boards. The boards were painted black to reduce optical reflections.

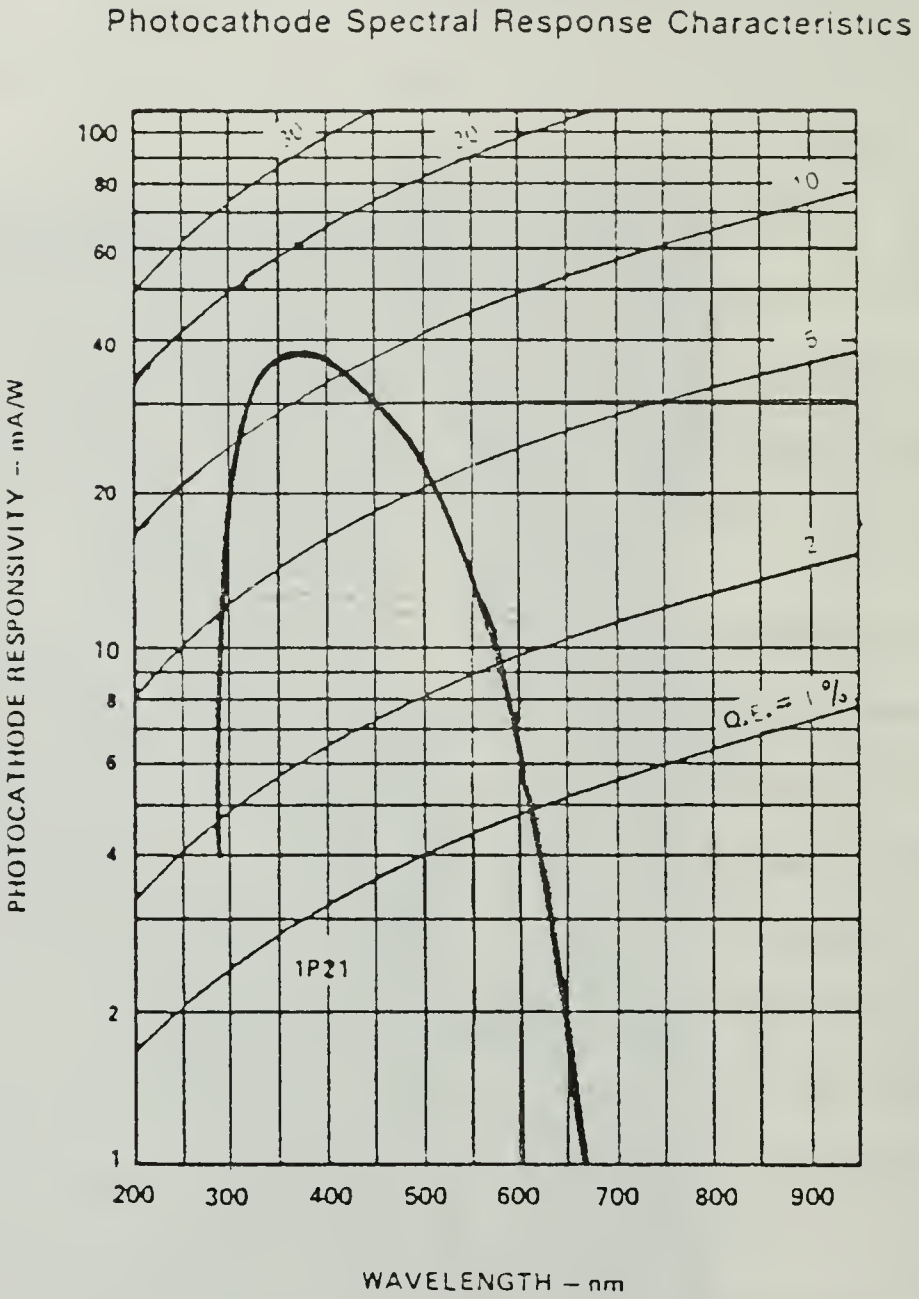

Figure 7. Quantum Efficiency for RCA 1P21 Photomultiplier

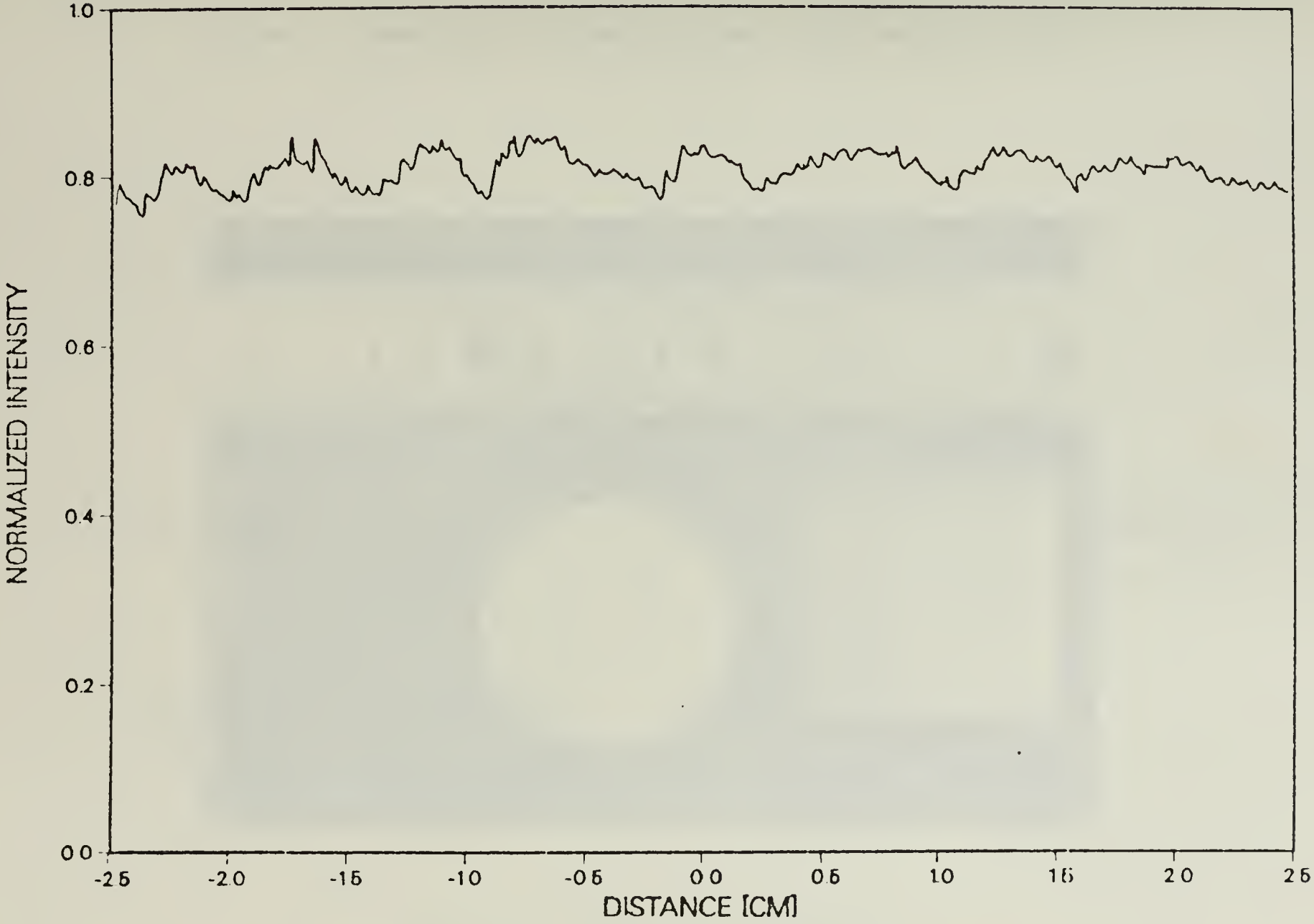

Figure 8. Intensity Measurement Using He-Ne Laser (4% Milk/Water Diffuser)

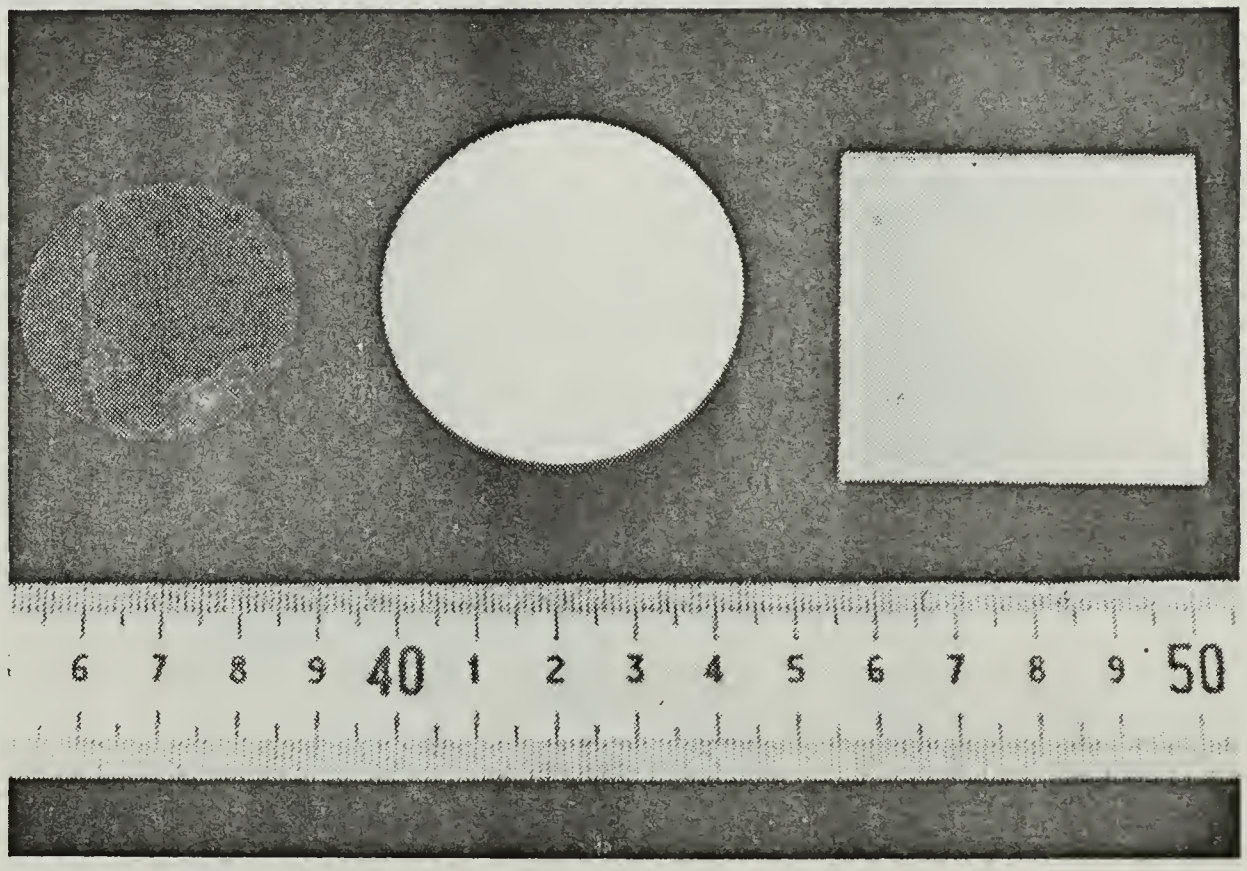

Figure 9. Ground Glass, Ground Glass/Opal Glass, and Opal Glass

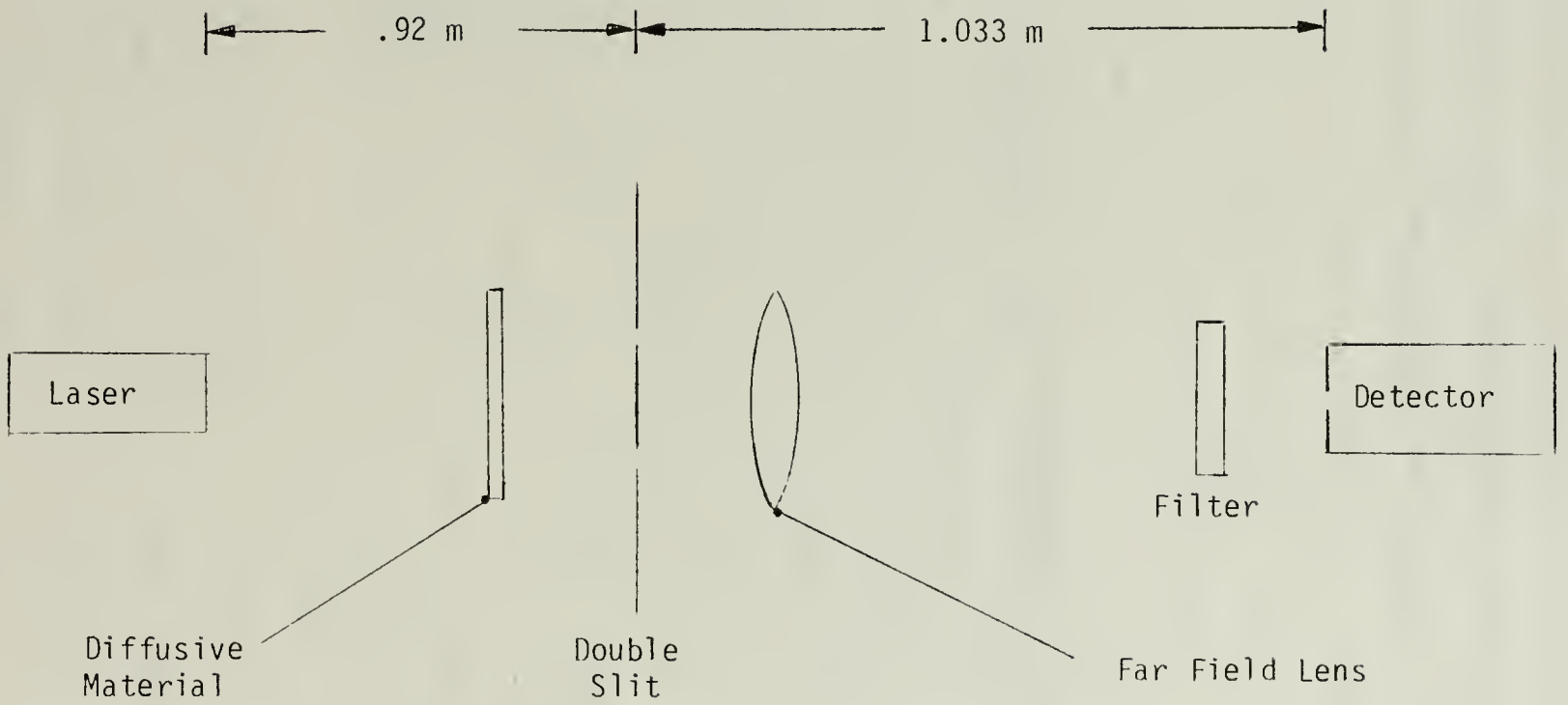

Figure 10. Diagram for Experiment #1

A far field lens was not included in the initial experimental set-up. The maximum spacing between the double slits and the photo-multiplier was 3.7 meters due to the limited size of the working area. An arbitrary boundary for the Fraunhofer region was determined using the Rayleigh range equation,

$$R = \frac{\pi w_o^2}{\lambda} , \qquad (16)$$

where w_o is the beam waist. For the argon ion laser with a .5 mm beam waist, the Rayleigh range is 6.4 meters. Therefore, a spacing of 3.7 meters does not satisfy the far field condition. Using mirrors to extend the separation between the slits and the photo-multiplier created alignment problems and introduced astigmatism. However, placing a convex lens with a 98.6 cm focal length after the double slit resolved the far field problem. In addition to ensuring Fraunhofer diffraction, the lens made it possible to plot the principal maximum as well as two subsidiary maxima of the diffraction pattern.

Placing the diffusive medium at different positions between the laser and the double slits altered the fringe visibility. Therefore, the coherence of the light vibrations from the slits changed since F.V.' = $|\gamma_{12}(\tau)|$ from eqn. 12.

The interference patterns were plotted on the X-Y recorder by slowly rotating the handle on the micrometer slide, thereby moving the photomultiplier across the observation plane. Several scans were necessary to adjust the photomultiplier voltage and to correct the alignment of the double slit and diffusive material. The overhead lights were turned off for each measurement. The zero baseline was obtained by covering the aperture on the cloth enclosure and making a measurement with the laser on, removing the effects of extraneous light from the experiment. Figures 11 through 18 show some examples of the interference patterns made for each diffusive medium placed at different intervals from the double slits. Tables 2 through 4 give a tabulation of the fringe visibility results for ground glass, opal/ground glass, and opal glass, respectively. The fringe visibility was calculated using eqn. 11. Figures 19 through 21 display plots[4] of the coherence versus distance to the double slits for ground glass, opal/ground glass, and opal glass. In each case there is a minimum in the curve. For opal glass this minimum occurs at 17 cm from the double slits and will be referred to as the "position of incoherence."

A modification of experiment #1 involves placing a collimating lens between the opal glass and the double slit.

---

[4]The curves connecting the data points were computer generated using an (N-1)-order polynomial fit, where N is the number of data points.

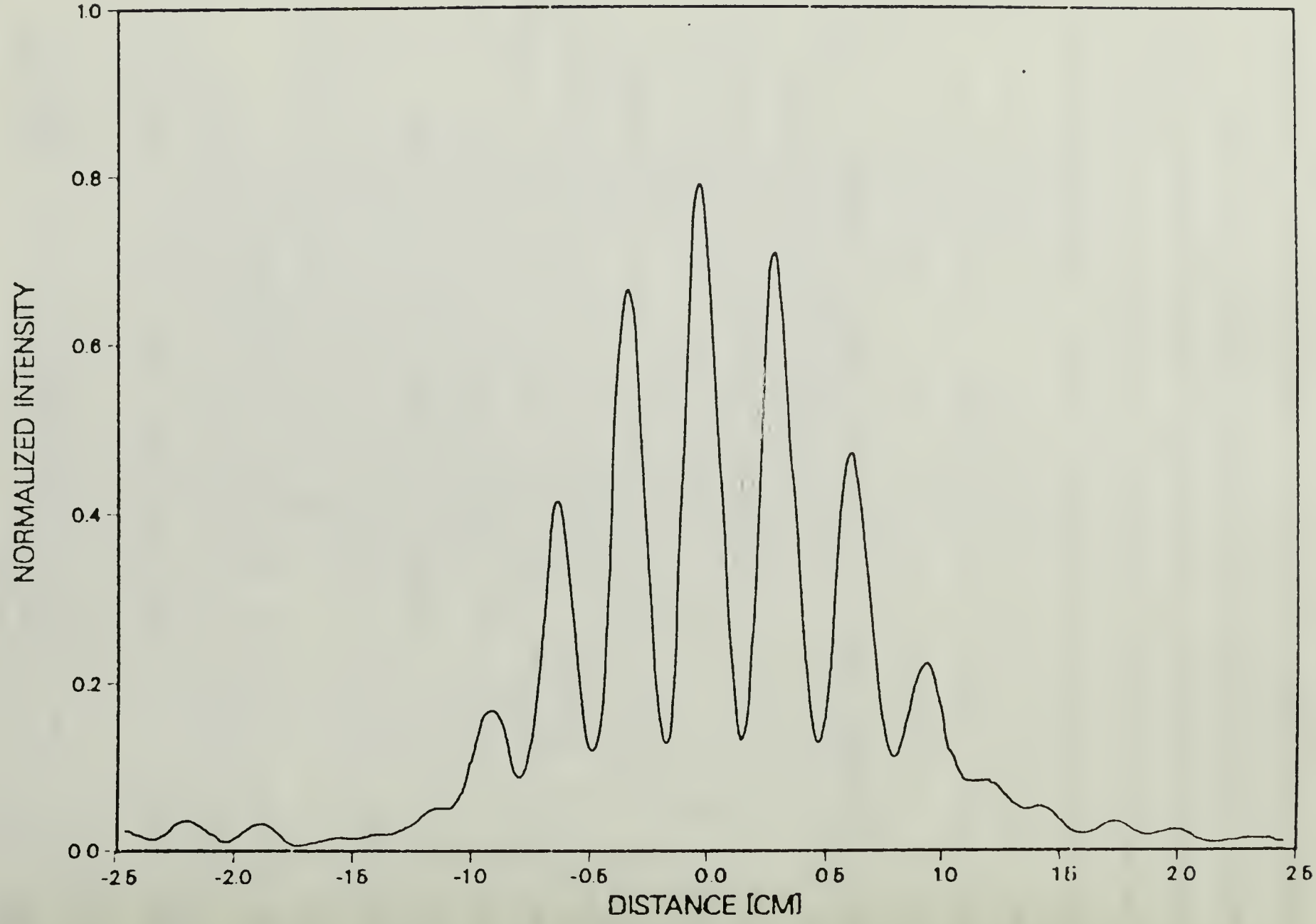

Figure 11. Interference Pattern for Ground Glass 10 cm from Slits

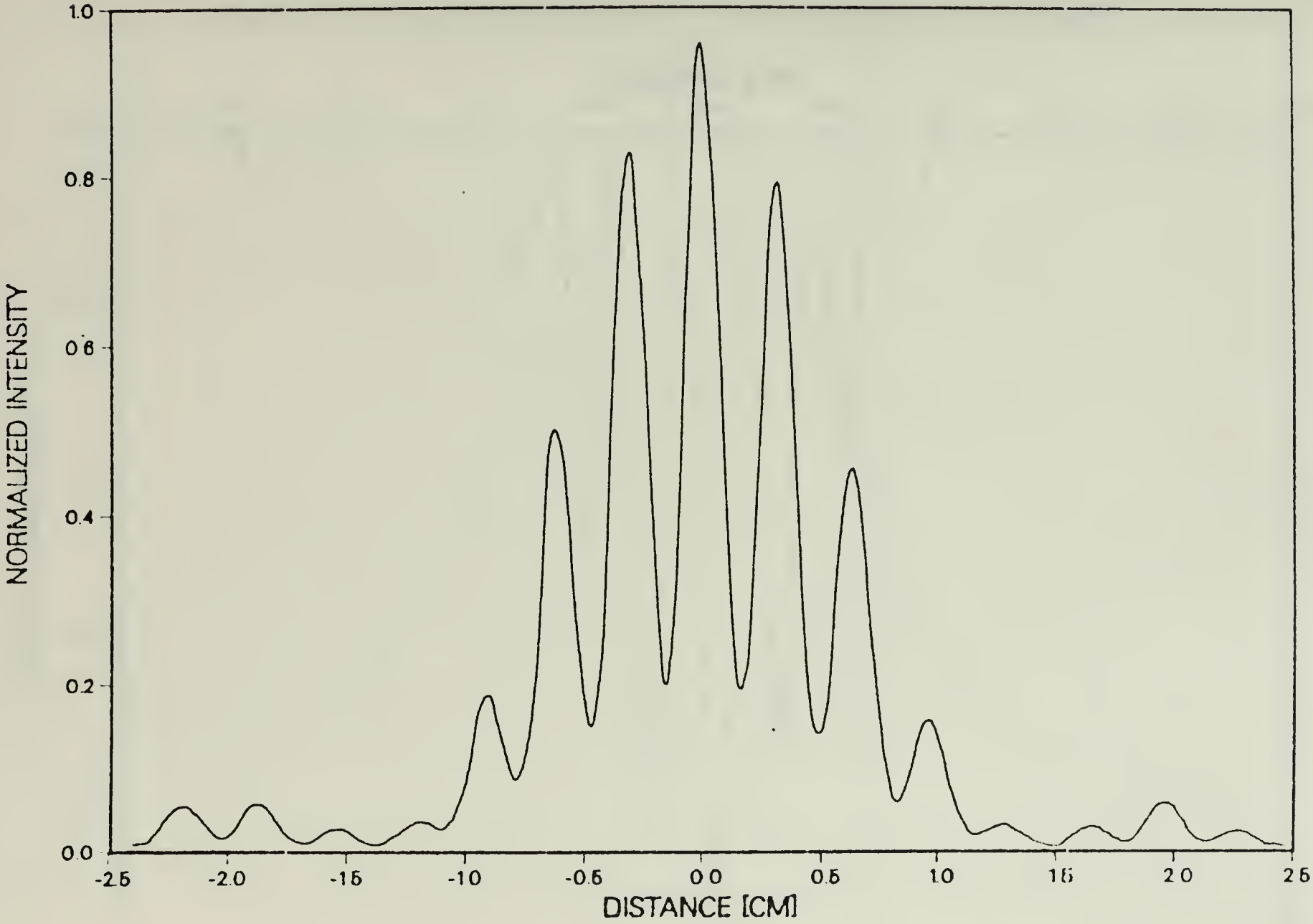

Figure 12. Interference Pattern for Ground Glass 30 cm from Slits

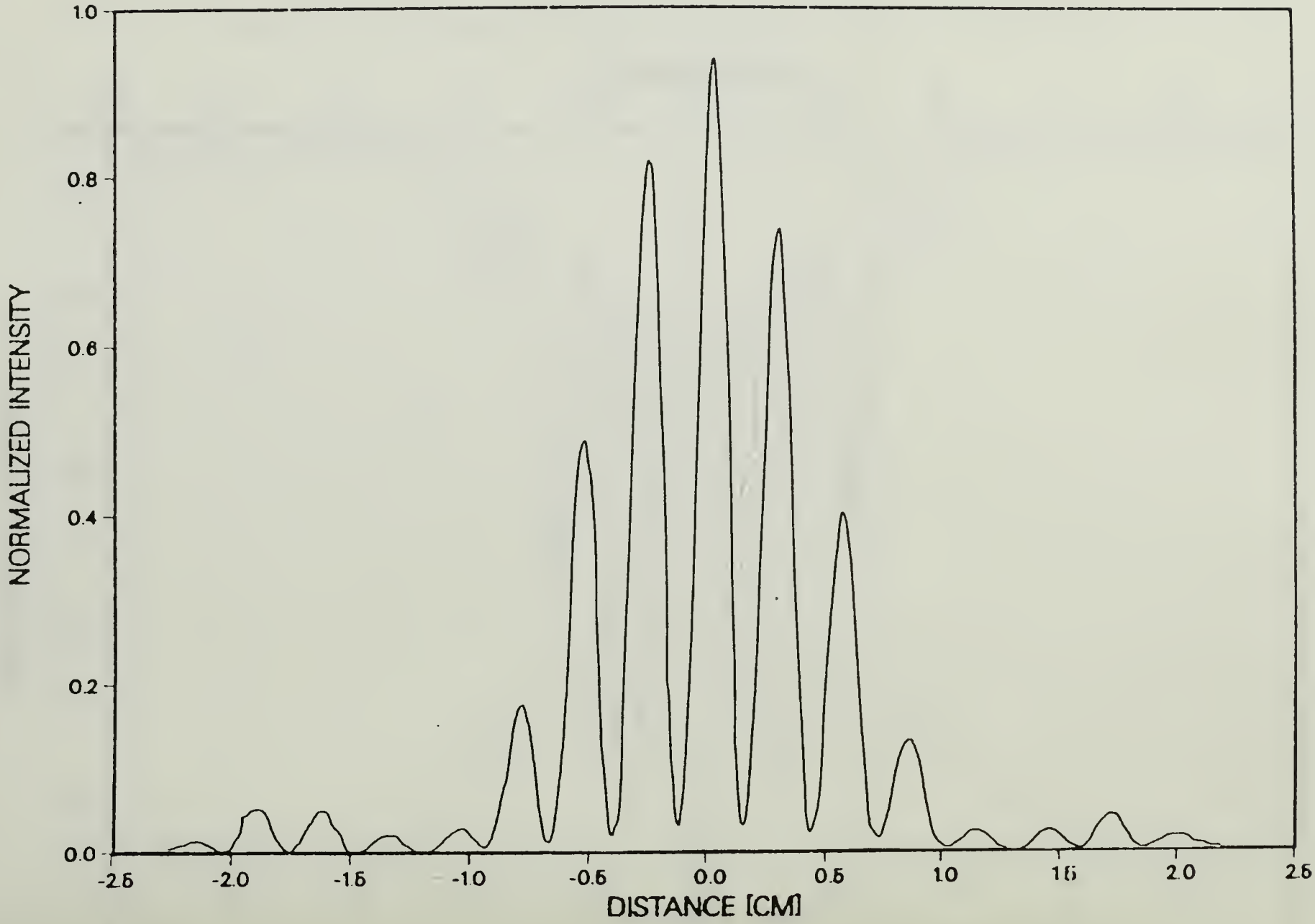

Figure 13. Interference Pattern for Ground Glass 60 cm from Slits

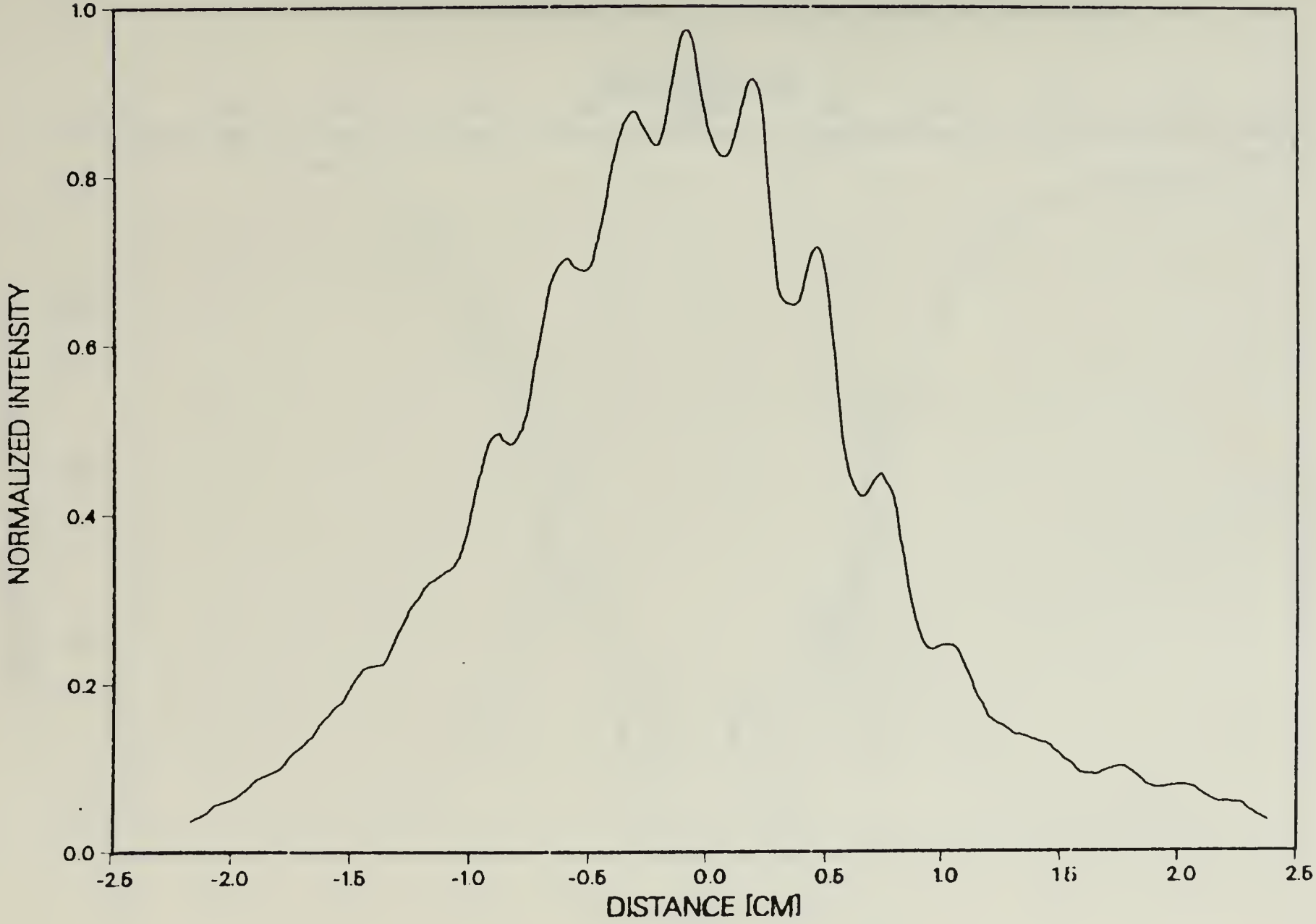

Figure 14. Interference Pattern for Opal/Ground Glass 20 cm from Slits

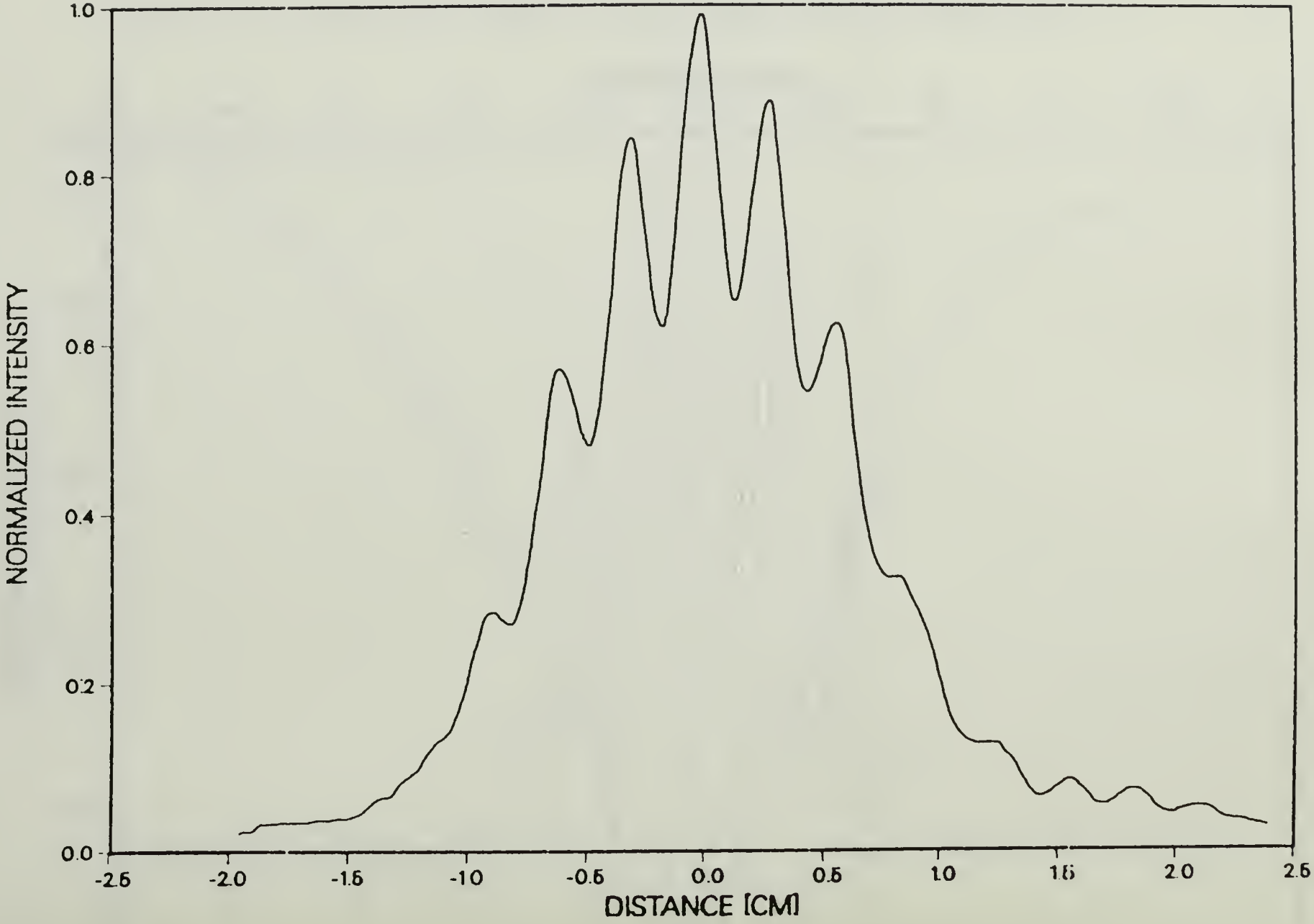

Figure 15. Interference Pattern for Opal Glass 15 cm from Slits

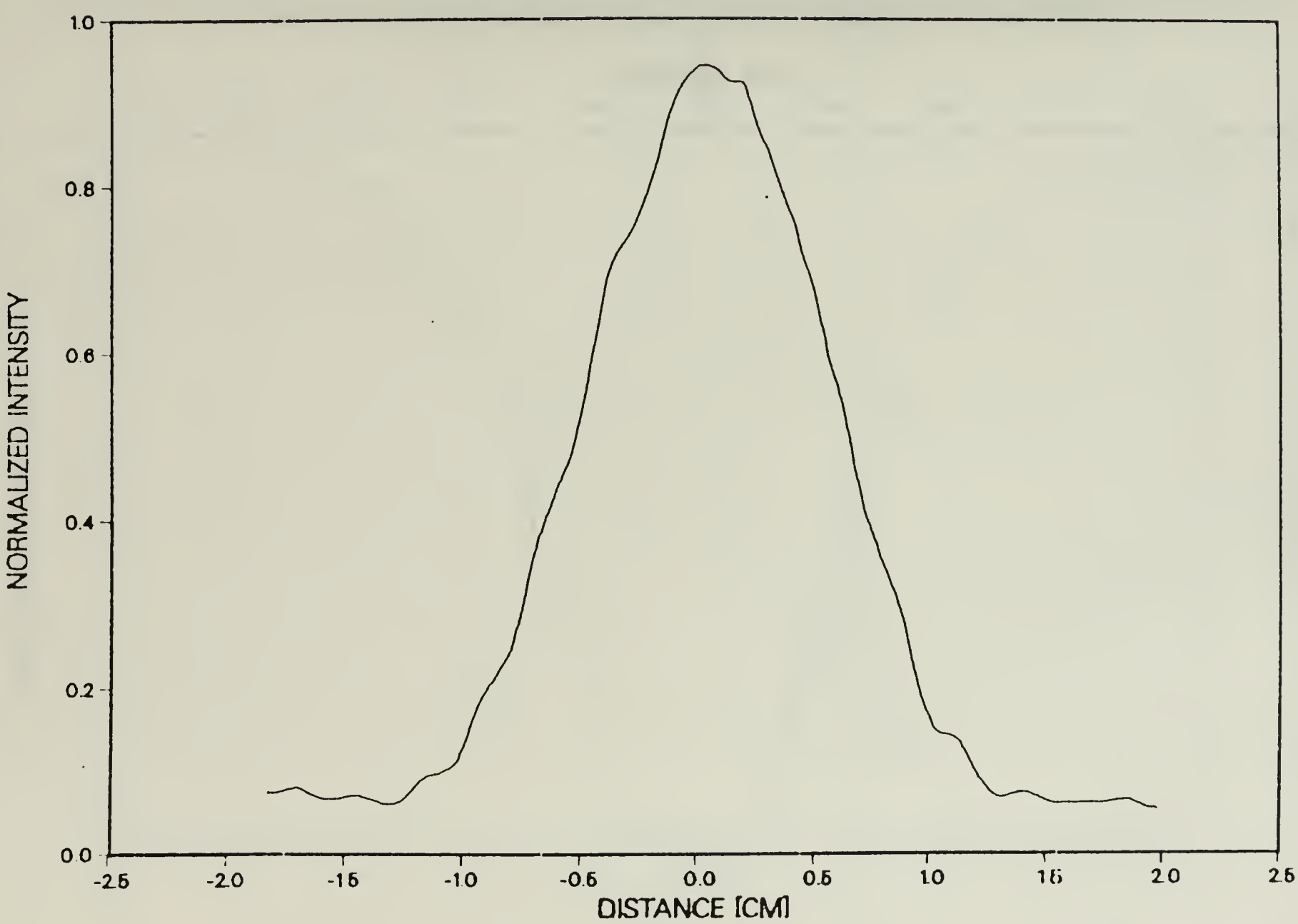

Figure 16. Interference Pattern for Opal Glass 17 cm from Slits

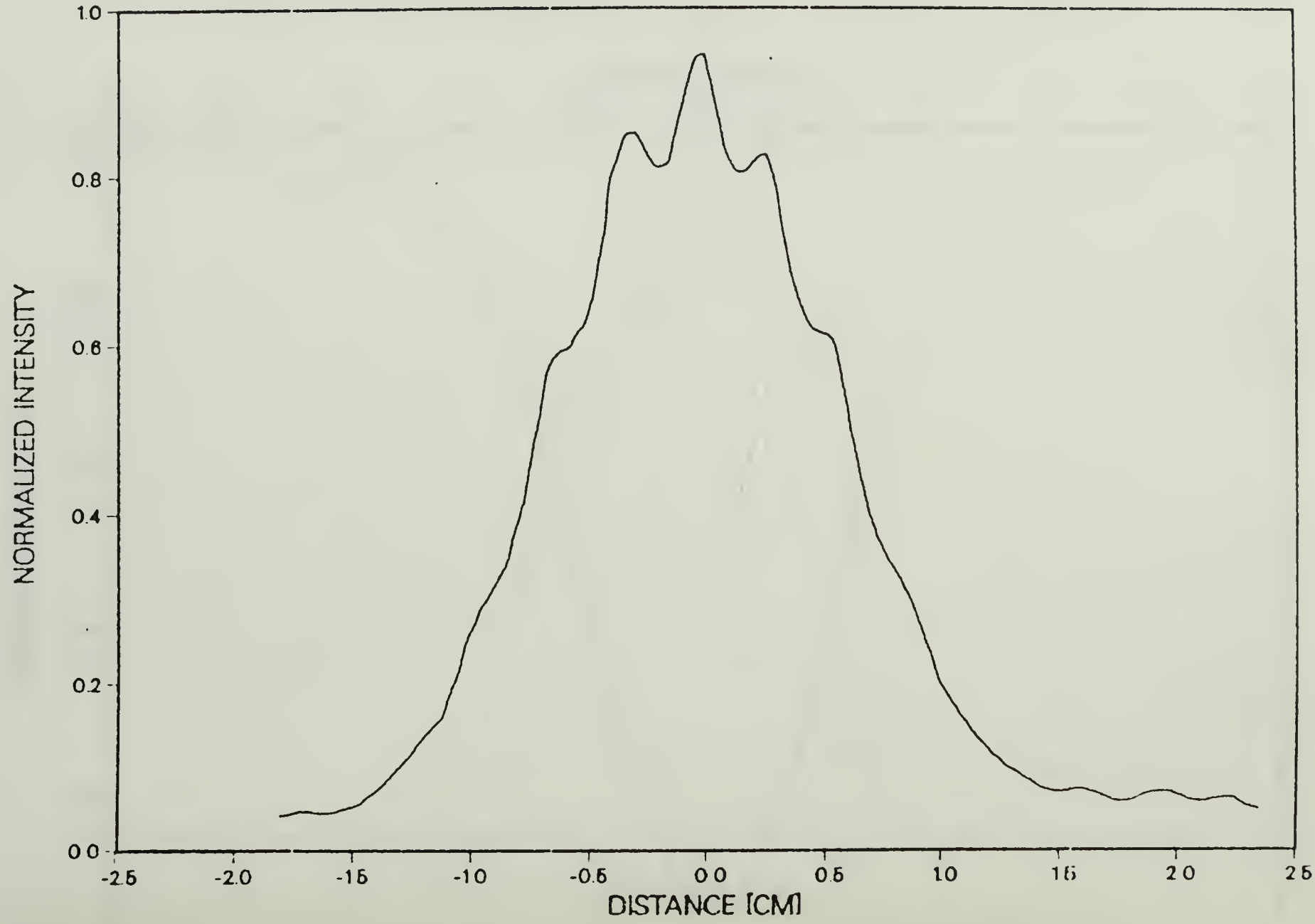

Figure 17. Interference Pattern for Opal Glass 18 cm from Slits

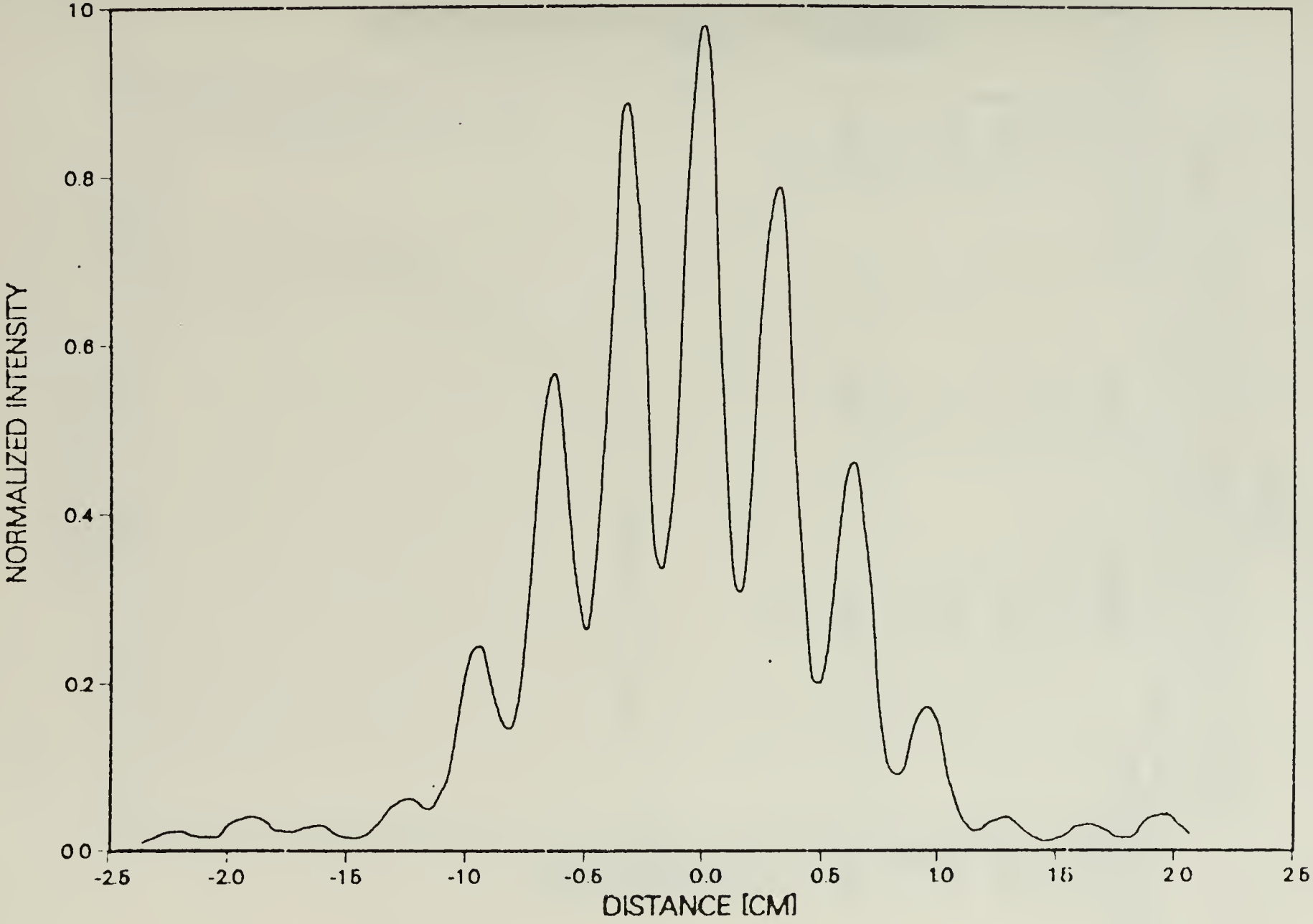

Figure 18. Interference Pattern for Opal Glass 40 cm from Slits

TABLE II

FRINGE VISIBILITY RESULTS FOR GROUND GLASS

Distance (cm)	I_{max}	I_{min}	Fringe Visibility
10	81.5	13	.725
20	110	15	.760
30	99	19	.678
40	126	10	.853
50	116	6.5	.894
* 60	111.5	4	.931

* Interference pattern reduced 7%.

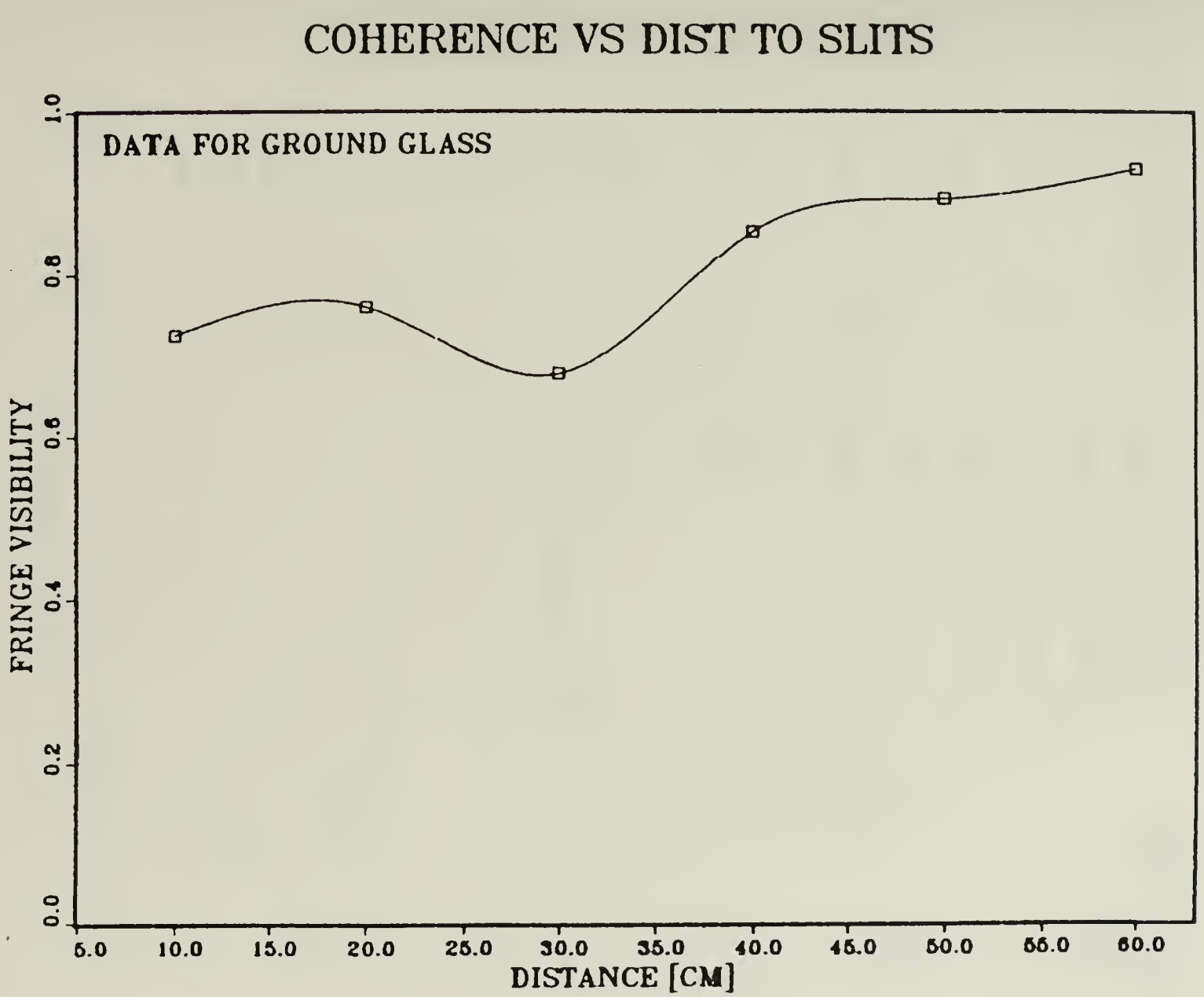

Figure 19. Plot of Coherence vs Distance for Ground Glass

TABLE III

FRINGE VISIBILITY RESULTS FOR OPAL GLASS/GROUND GLASS

Distance (cm)	I_{max}	I_{min}	Fringe Visibility
18	104	89	.078
19	119	100	.087
19.5	110.5	96.5	.068
* 20	94.5	86.5	.044
21	110	85.5	.125
30	113	81	.165
40	112.5	58.5	.316

* Interference pattern reduced 7%.

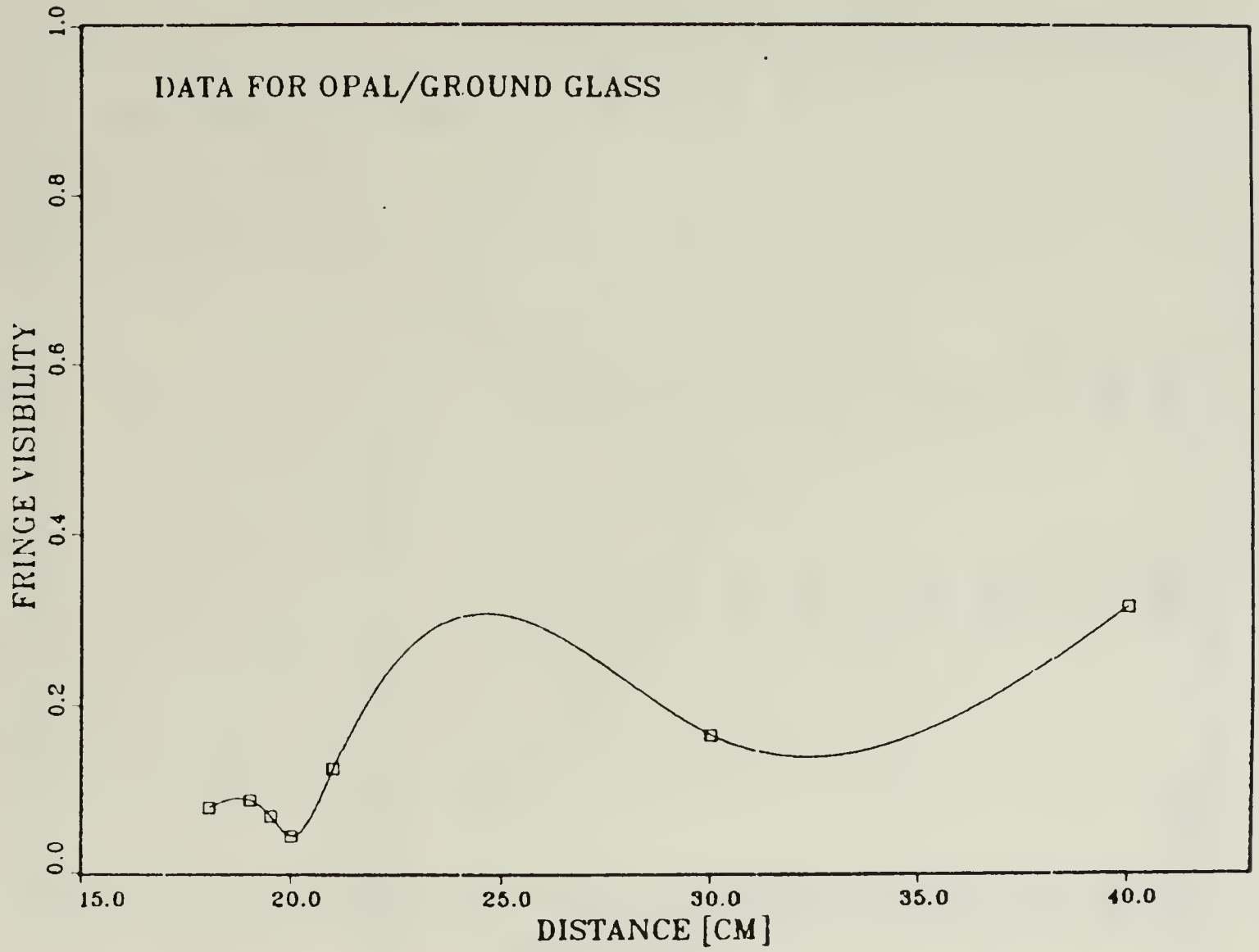

Figure 20. Plot of Coherence vs Distance for Opal/Ground Glass

TABLE IV

FRINGE VISIBILITY RESULTS FOR OPAL GLASS

Distance (cm)	I_{max}	I_{min}	Fringe Visibility
10	111	86.5	.124
* 15	110	70.5	.219
* 17	111	110	.004
18	97	83	.078
20	107	86.5	.106
25	103.5	85	.098
30	112	72.5	.214
40	104	35.5	.491
50	109	34	.524
60	109.5	27.5	.598

* Interference pattern reduced 7%.

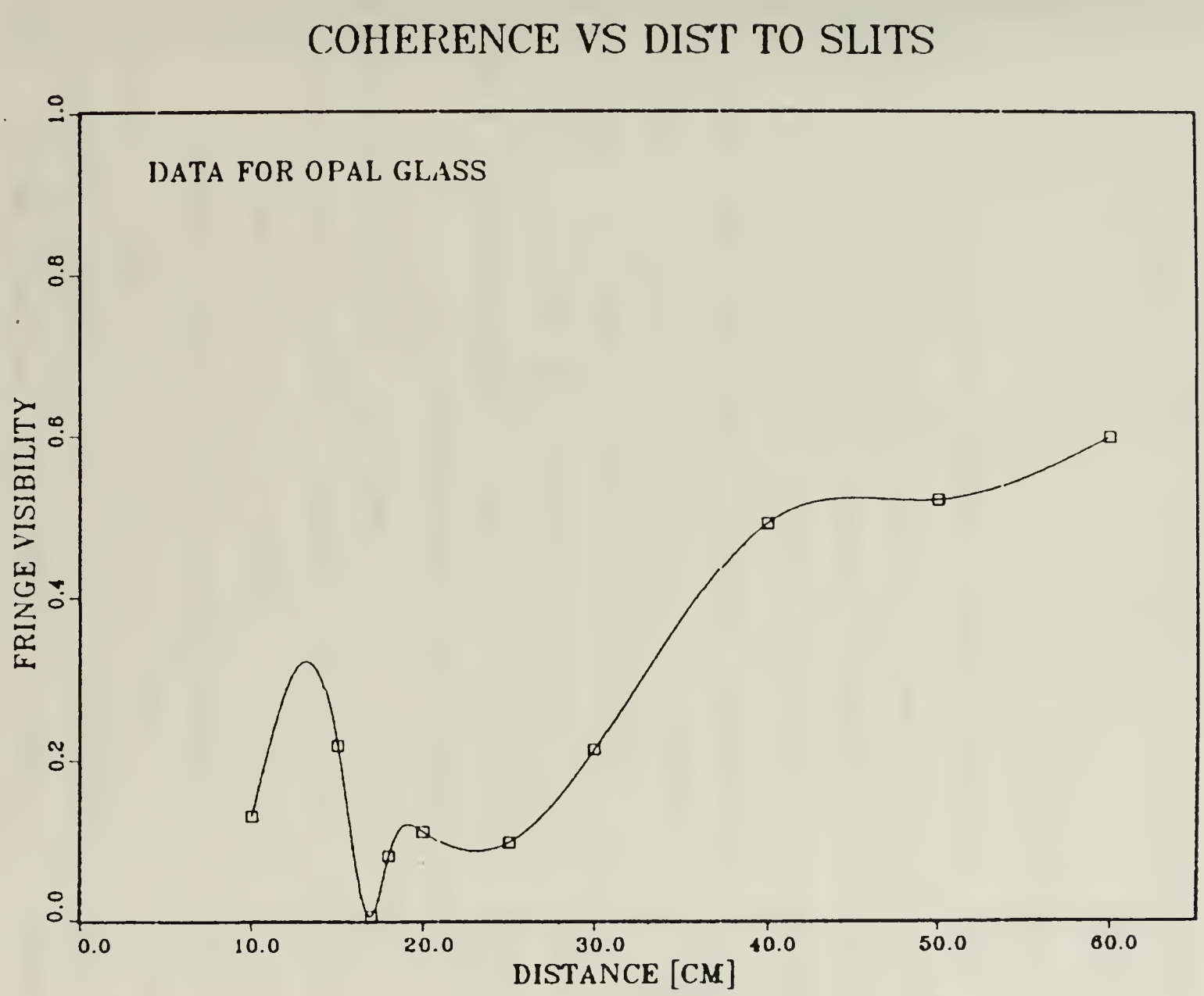

Figure 21. Plot of Coherence vs Distance for Opal Glass

Figure 22 shows the interference pattern for the lens and opal glass placed at 30 cm and 35 cm, respectively, from the double slit. The pattern shows a significant amount of coherence degradation, however, the factors contributing to the triangular shape of the interference pattern are unknown.

C. EXPERIMENT #2

The geometrical significance of the spacing between the double slits and the diffusive material was investigated by replacing the diffusive material with a single slit. Figure 23 shows the interference pattern with the single slit 30 cm from the double slits. Table 5 shows the fringe visibility results and Figure 24 is a graph of coherence vs. single slit distance from the double slits. From this graph it is evident that the coherence remains high for all slit positions although the coherence increases slightly with increasing distance from the double slits.

A modification of this experiment involves replacing the single slit with a pinhole made by tapping a small hole in a piece of sheet metal. Figures 25 and 26 are samples of the interference patterns made with the pinhole placed at various distances from the double slits. Table 6 lists the fringe visibility results and Figure 27 shows a graph of coherence vs. pinhole distance from the double slits. The position of the pinhole affects the coherence and produces a

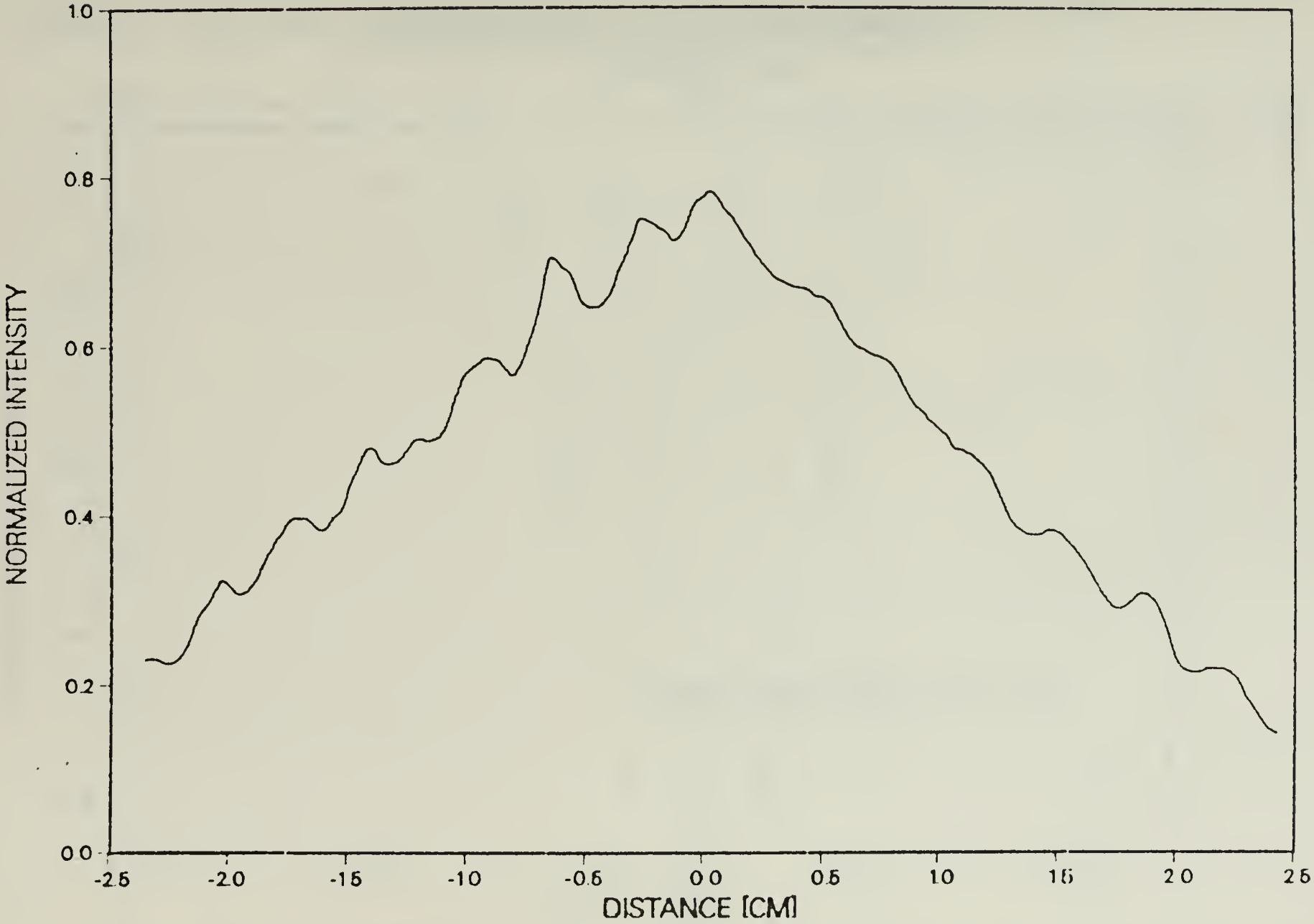

Figure 22. Interference Pattern with Collimating Lens Between Opal and Double Slit

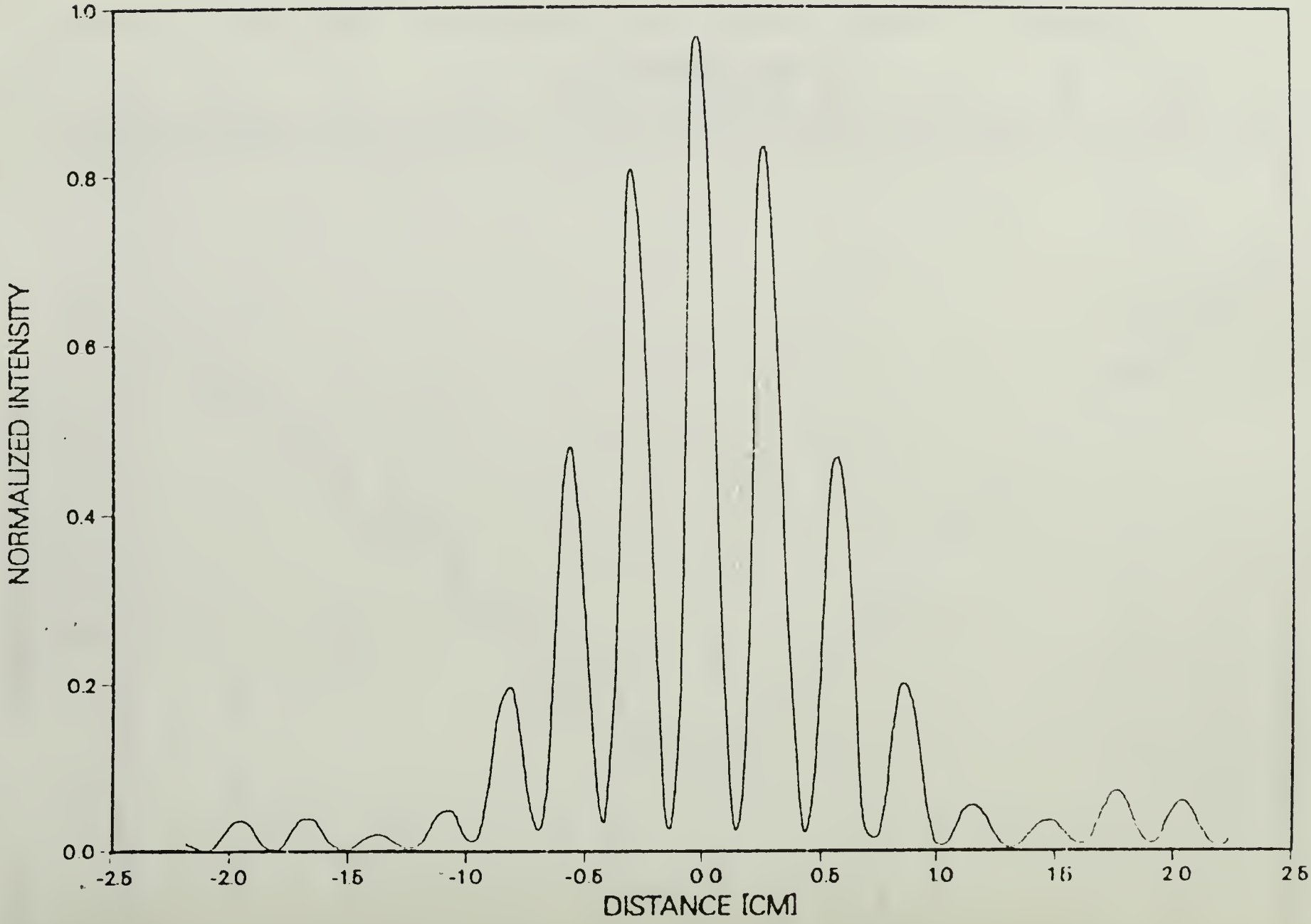

Figure 23. Interference Pattern for Single Slit 30 cm from Double Slit

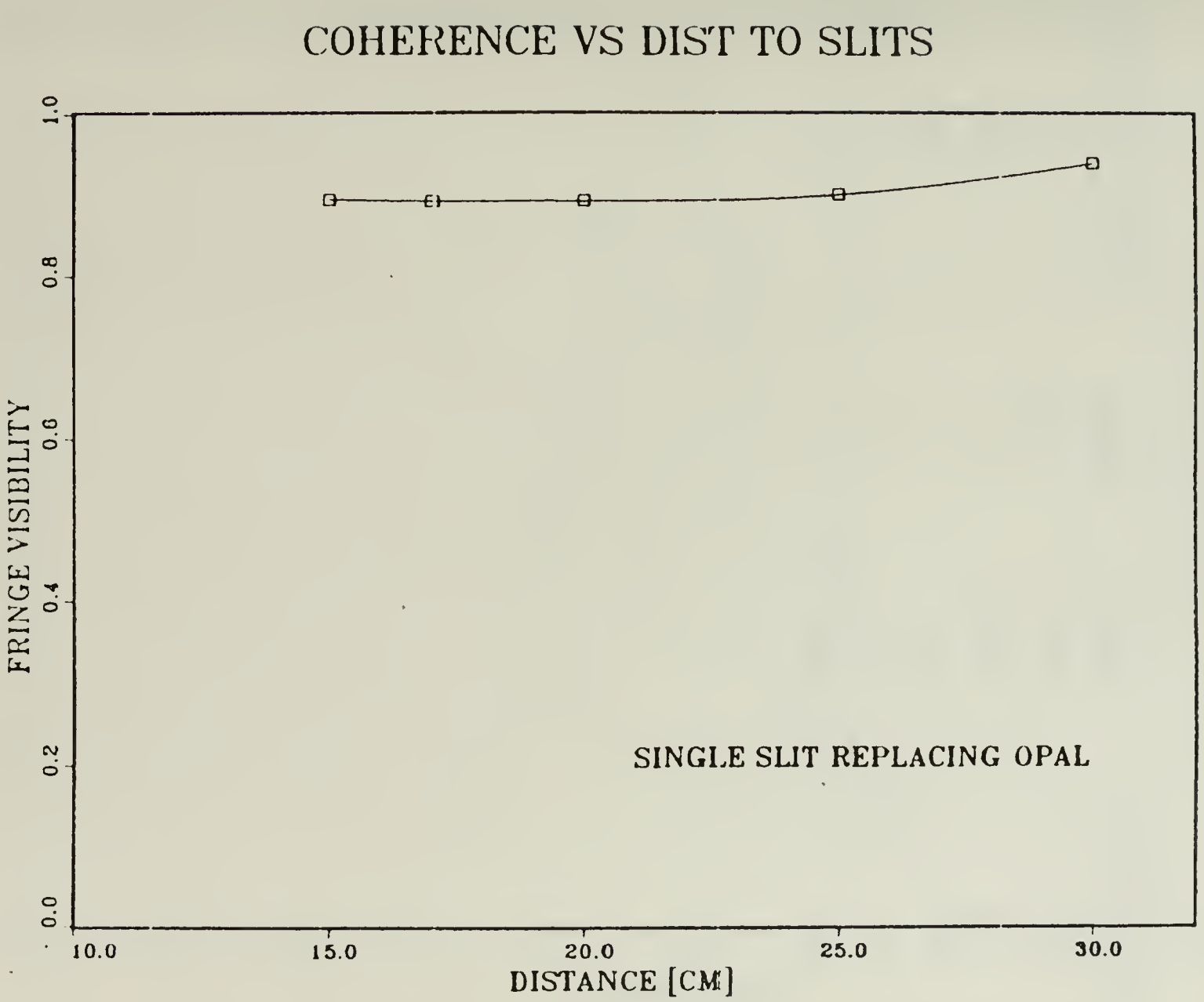

Figure 24. Plot of Coherence vs Distance for Single Slit

TABLE V

FRINGE VISIBILITY RESULTS FOR SINGLE SLIT
REPLACING DIFFUSIVE MATERIAL

Distance (cm)	I_{max}	I_{min}	Fringe Visibility
15	114	6.5	.892
17	105.5	6	.892
20	124	7	.893
25	115	6	.901
30	100	3	.94

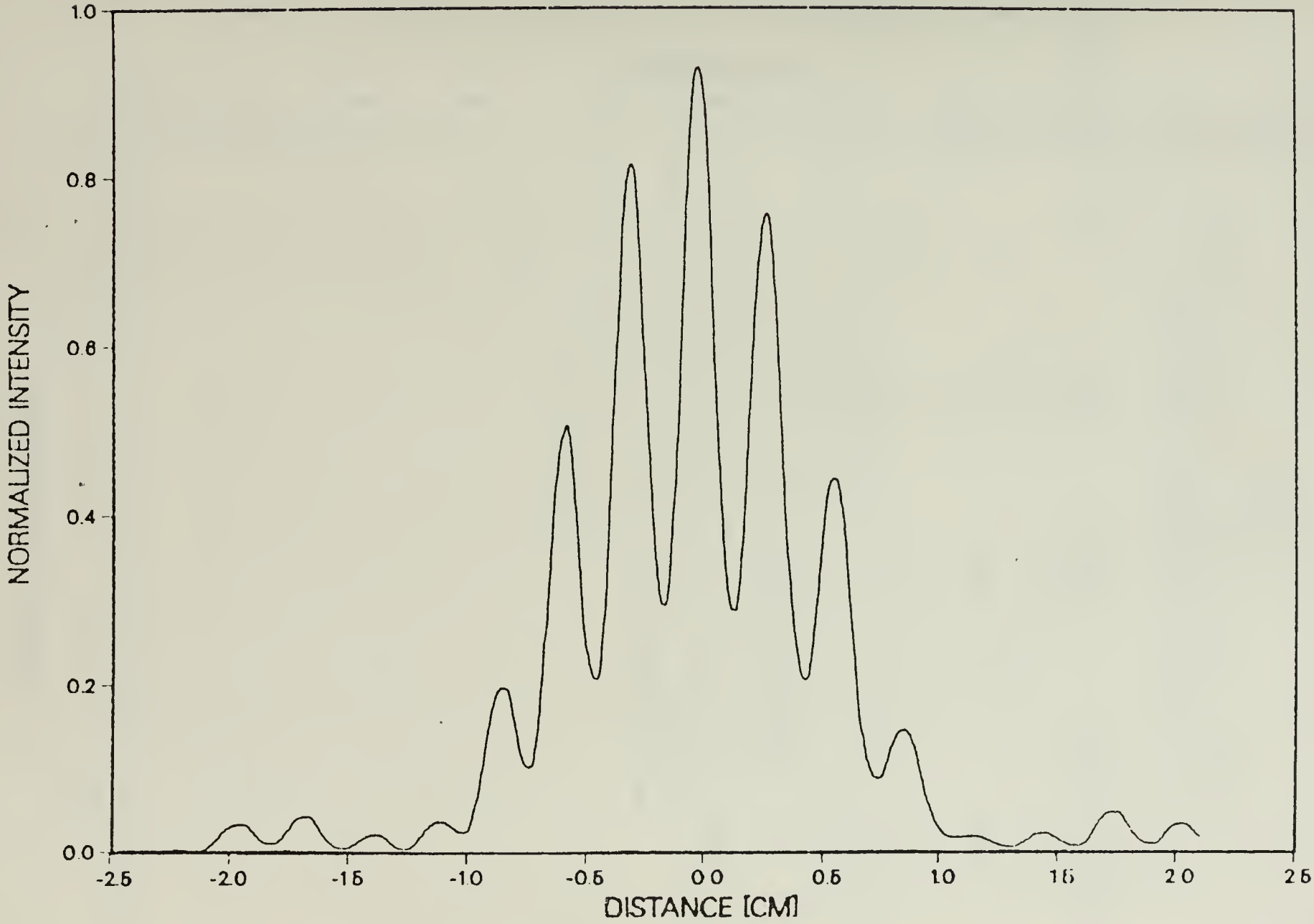

Figure 25. Interference Pattern for Pinhole 10 cm from Double Slit

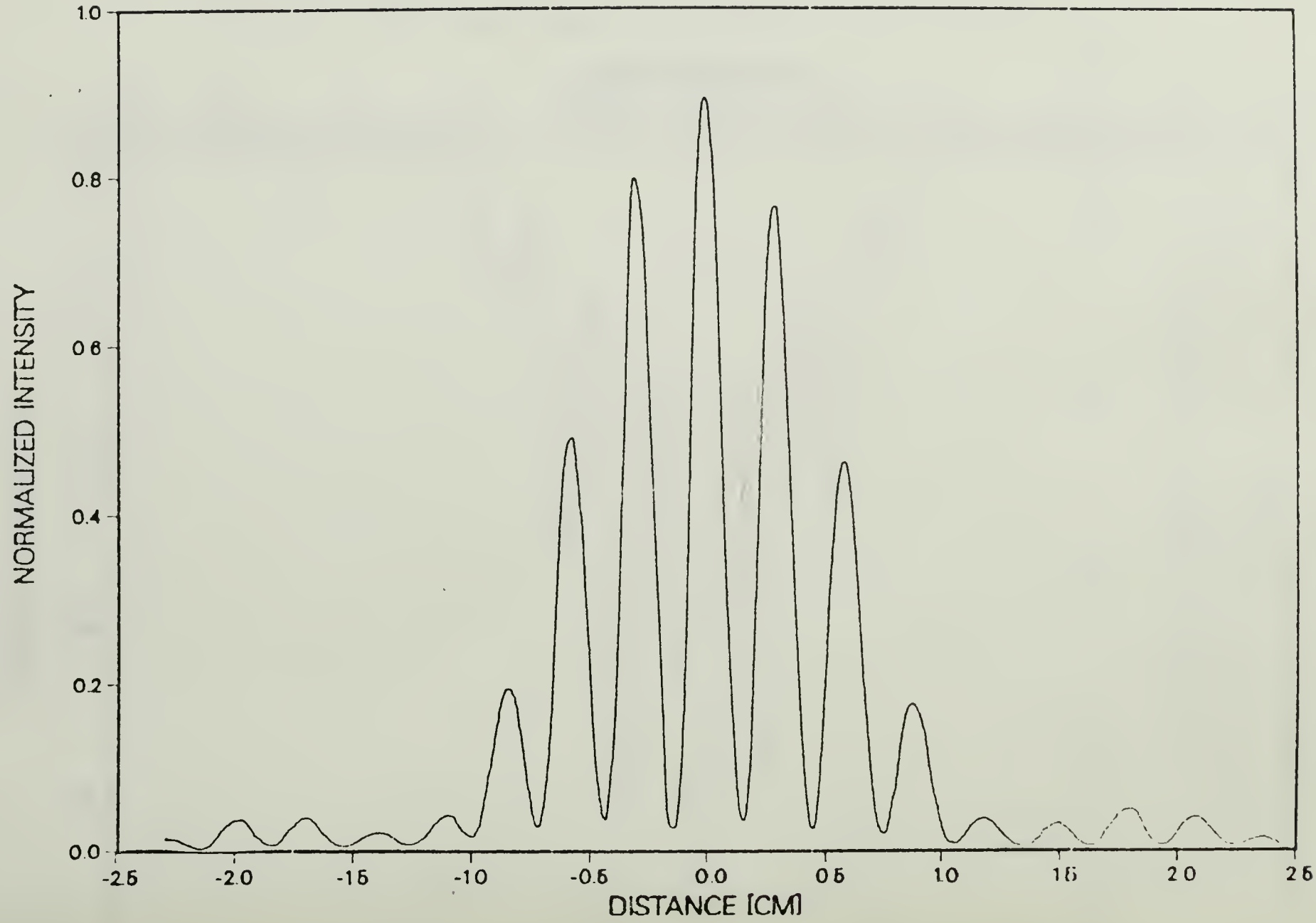

Figure 26. Interference Pattern for Pinhole 25 cm from Double Slit

TABLE VI

FRINGE VISIBILITY RESULTS FOR PINHOLE
REPLACING DIFFUSIVE MATERIAL

Distance (cm)	I_{max}	I_{min}	Fringe Visibility
10	97	30.5	.522
17	111	30.5	.569
19	114	31	.572
20	87.5	13	.740
25	92	3.5	.927
30	99.5	13.5	.761

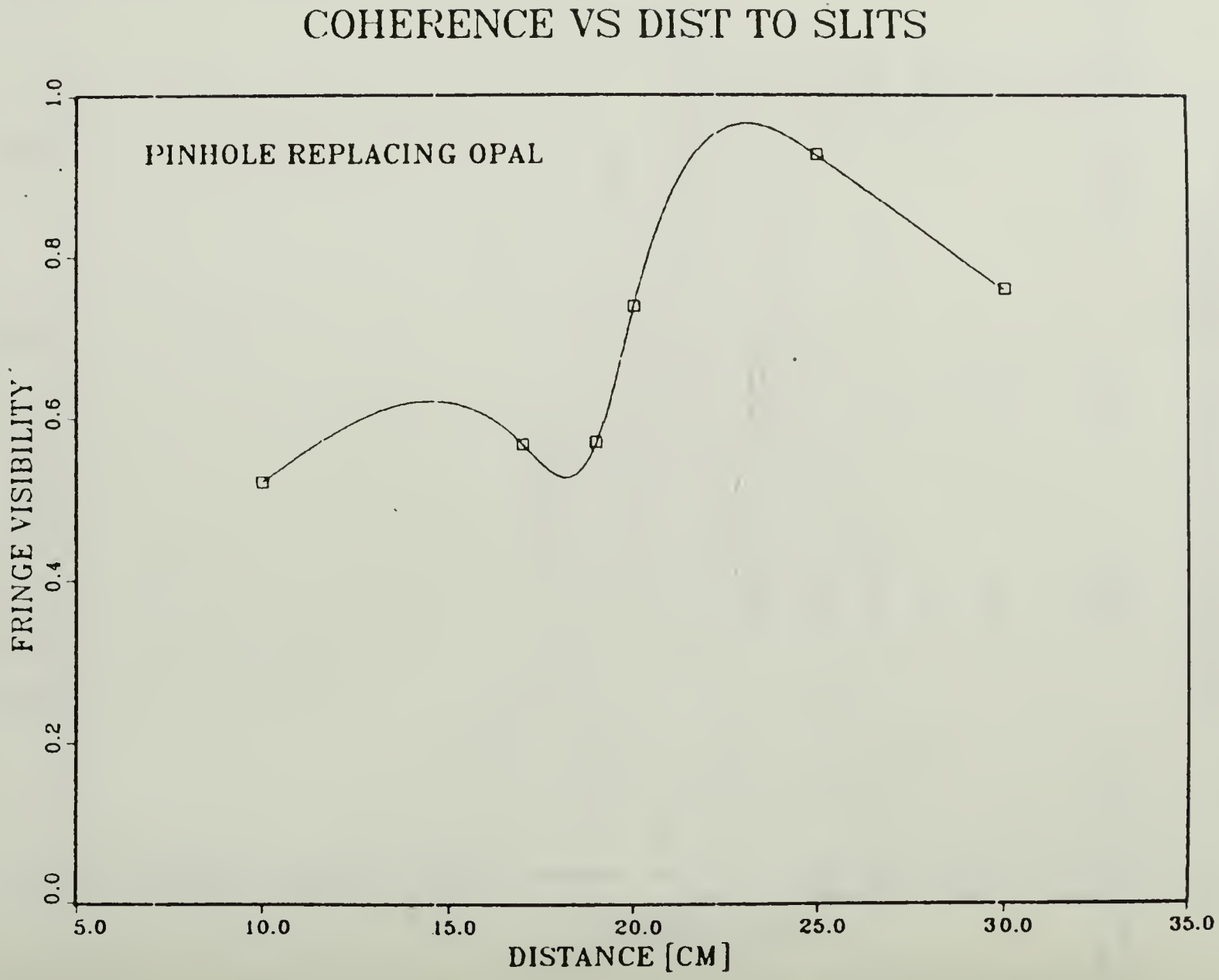

Figure 27. Plot of Coherence vs Distance for Pinhole

dip at 18 cm that is similar to the opal data results in Figure 21.

D. EXPERIMENT #3

The spot size of the laser beam on the diffusive material is another geometrical factor that might influence the location of the "position of incoherence" of the diffusive medium. The significance of the beam size was investigated by using two different positive lens configurations to increase the beam diameter from 1.5 mm to 2.9 mm and from 1.5 mm to 3.6 mm. This was accomplished by placing a beam expander between the laser and opal glass.

A measurement of the beam diameter was made by placing the photomultiplier tube at the double slit position and removing the double slits. Figures 28 and 29 show the Gaussian profiles for the 1.5 mm beam and the 2.9 mm beam, respectively. The horizontal line indicates the e^{-2} intensity position used to measure the beam diameter.

Figures 30 through 33 show some samples of the interference patterns for opal in the expanded beams at various positions from the double slits. Table 7 lists the fringe visibility results and Figure 34 shows a graph of the coherence of opal in a 2.9 mm beam as a function of distance to the double slits. Table 8 lists the fringe visibility calculations and Figure 35 shows a graph of the coherence for opal in a 3.6 mm beam at various distances from the double slits.

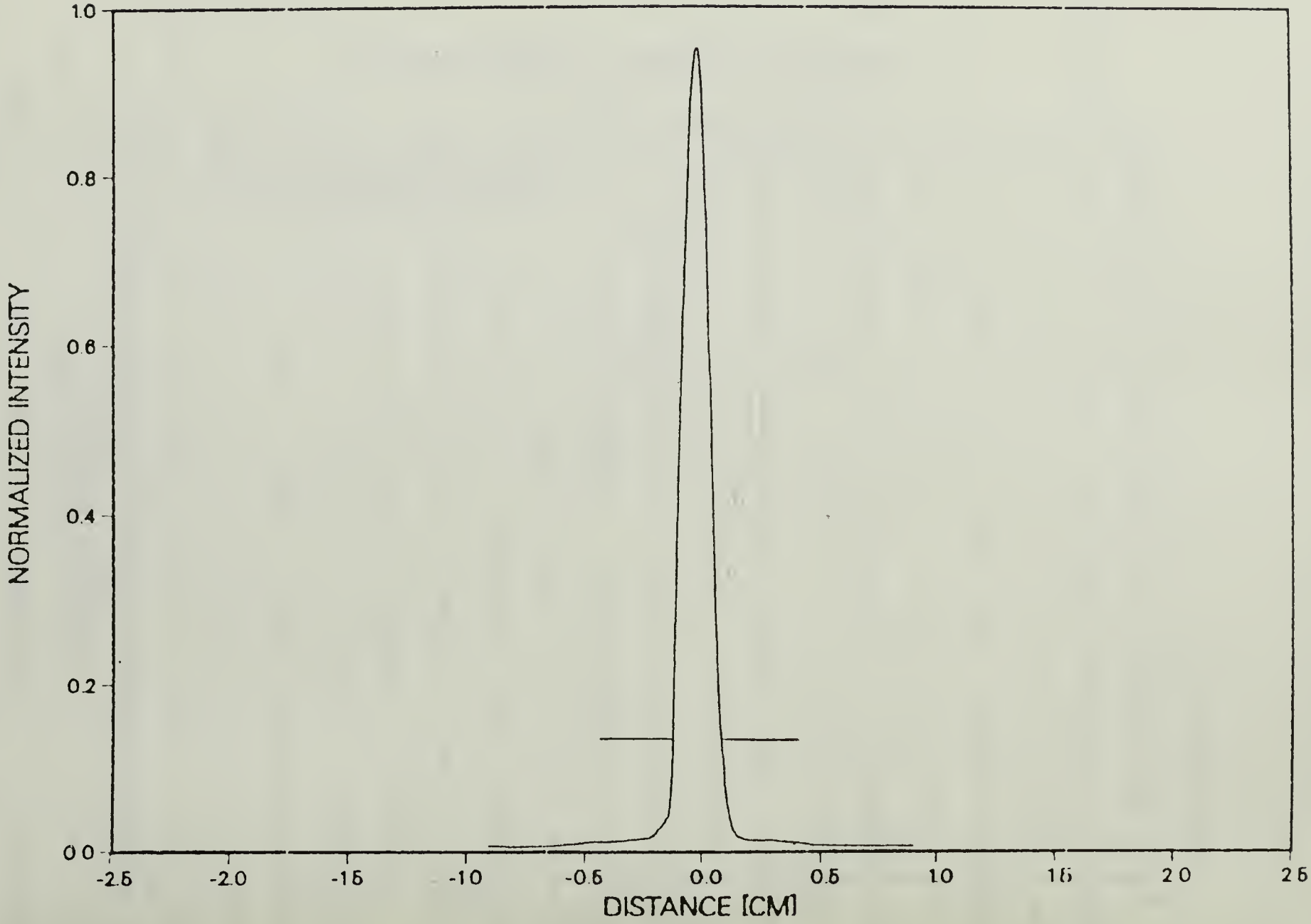

Figure 28. Gaussian Profile for Raw Laser Beam (1.5 mm)

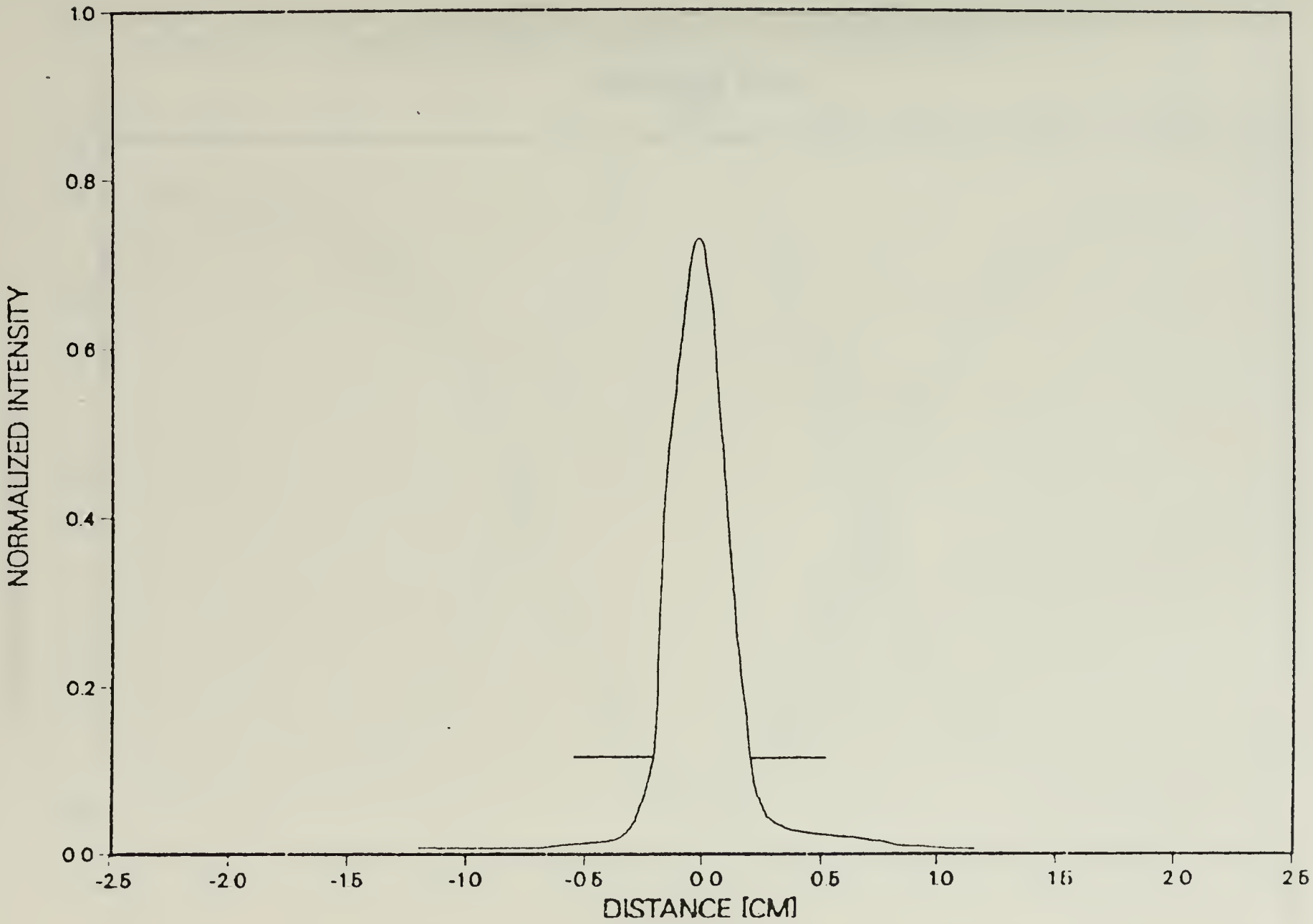

Figure 29. Gaussian Profile for 2.9 mm Diameter Beam

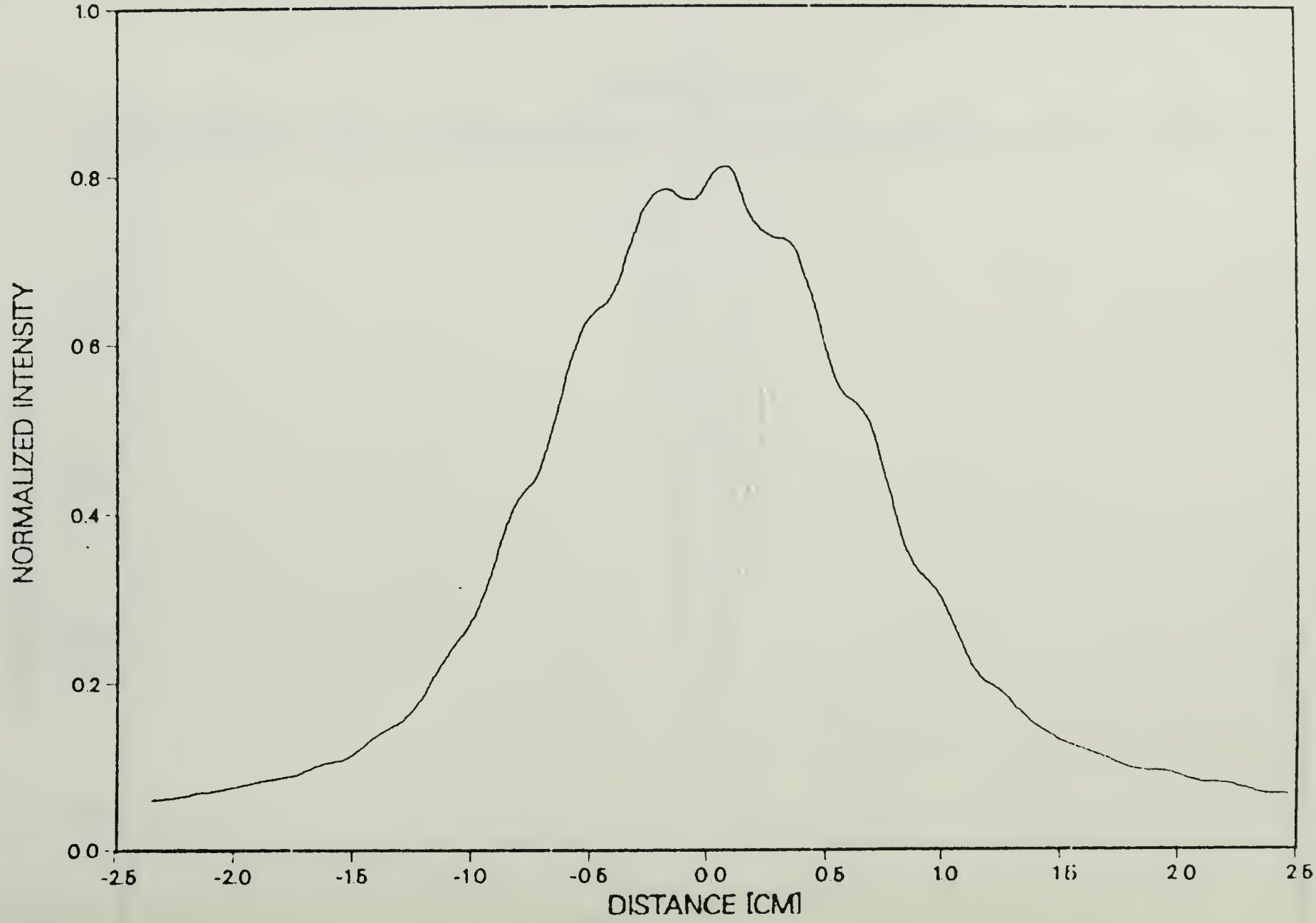

Figure 30. Interference Pattern for Opal at 17 cm (2.9 mm Beam)

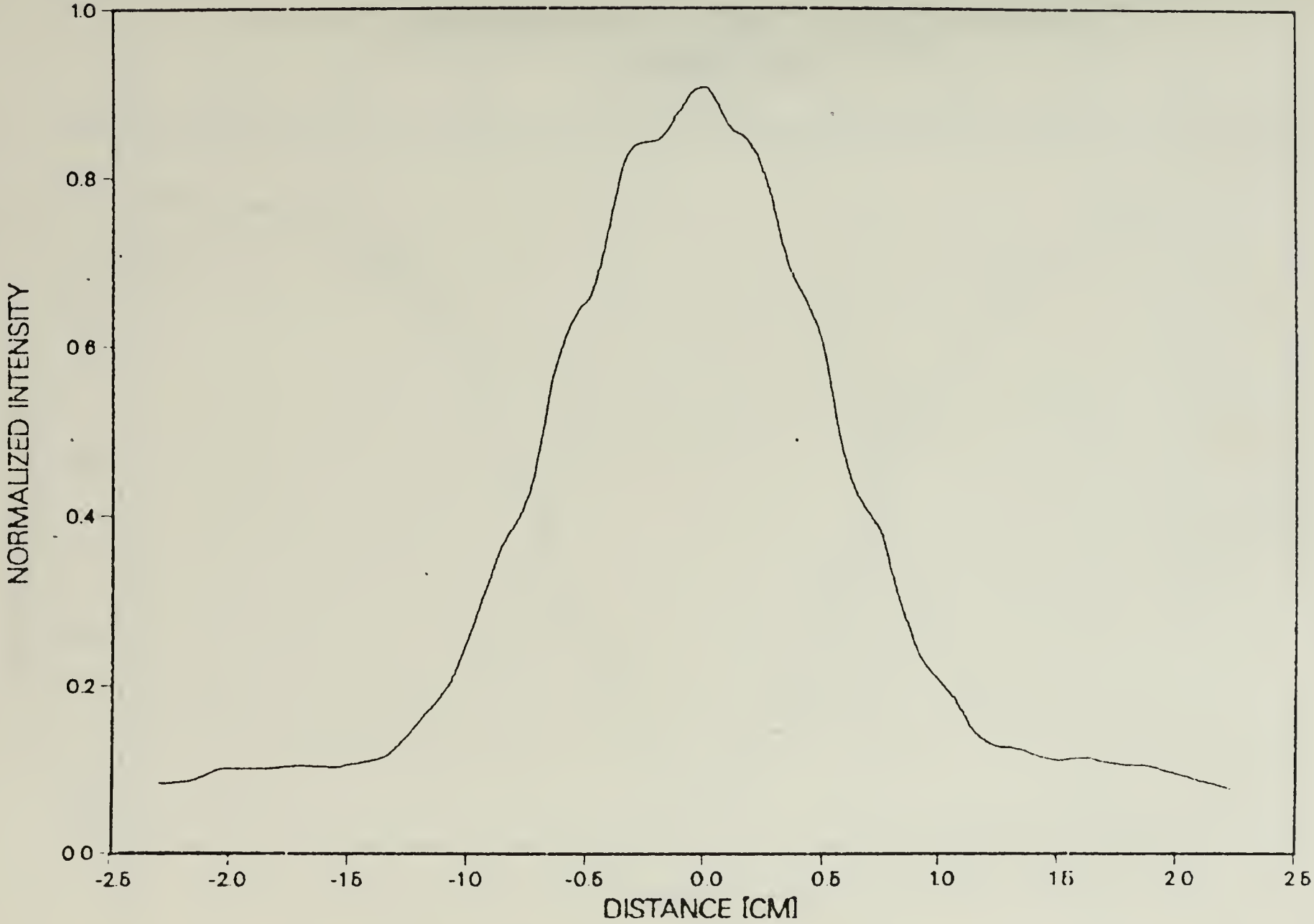

Figure 31. Interference Pattern for Opal at 30 cm (2.9 mm Beam)

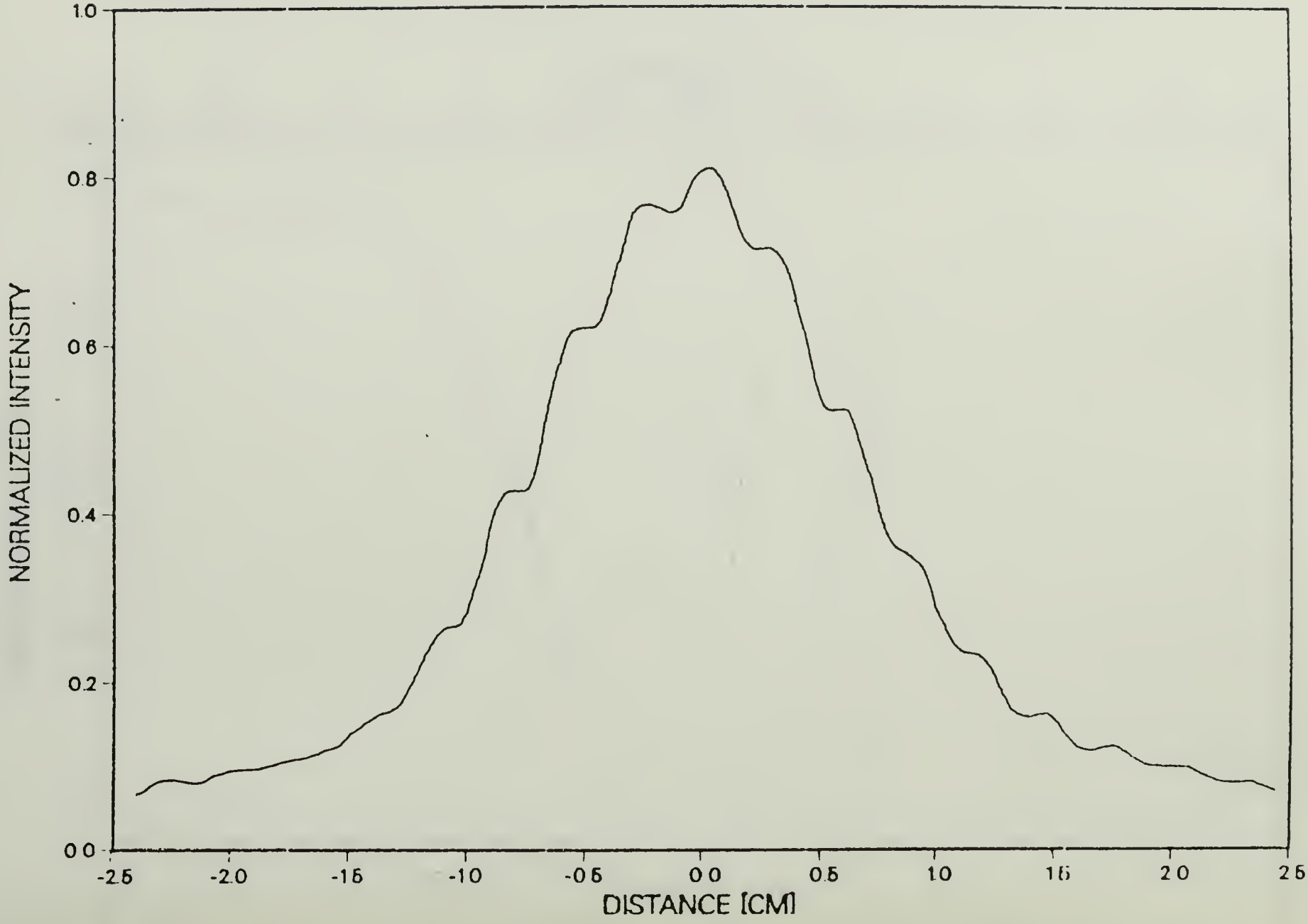

Figure 32. Interference Pattern for Opal at 21 cm (3.6 mm Beam)

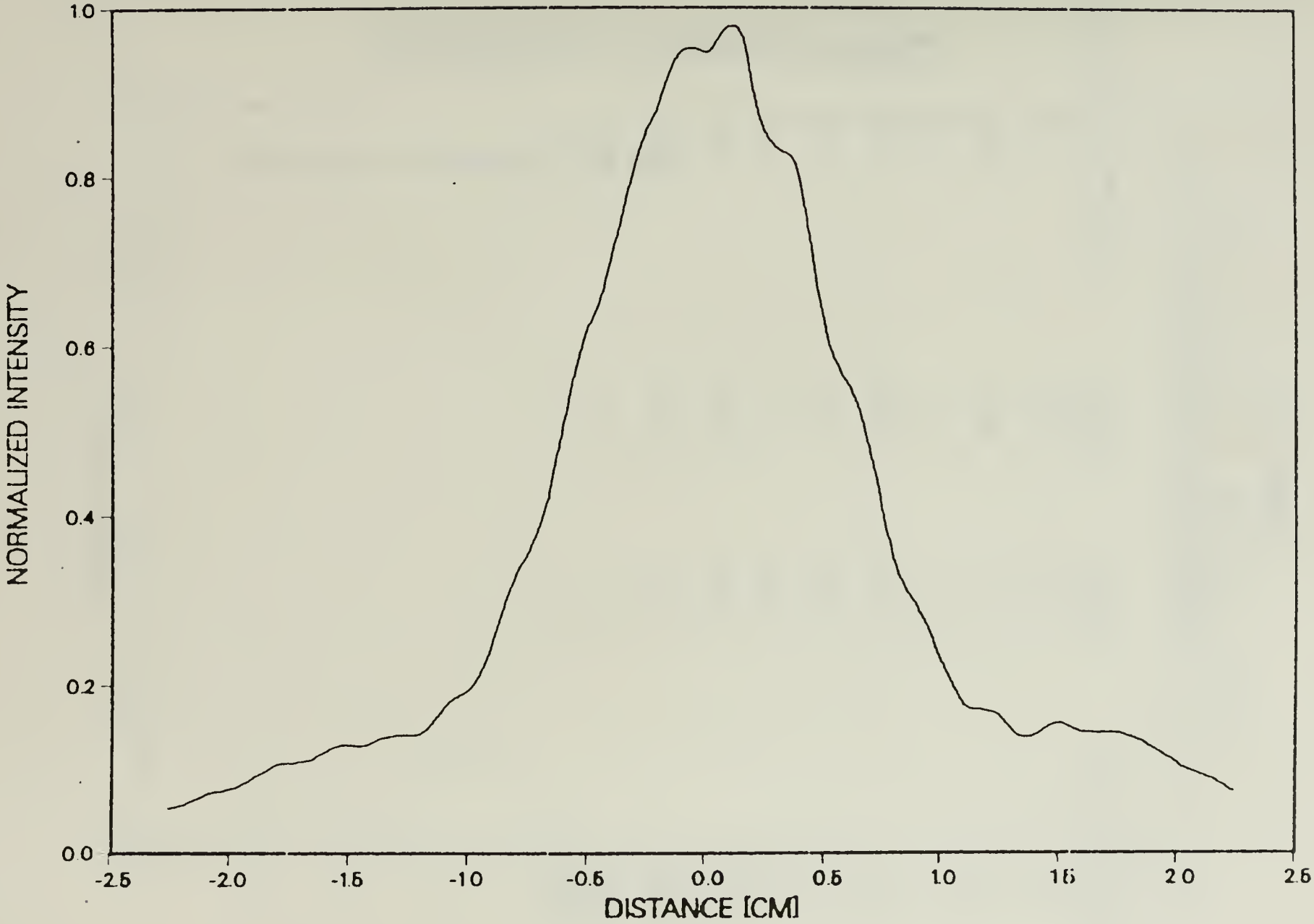

Figure 33. Interference Pattern for Opal at 40 cm (3.6 mm Beam)

TABLE VII

FRINGE VISIBILITY RESULTS FOR OPAL GLASS IN A 2.9 MM BEAM

Distance (cm)	I_{max}	I_{min}	Fringe Visibility
10	89.5	79	.062
15	90	80	.059
17	84	77	.044
20	88.5	67.5	.135
25	82.5	75	.048
30	93.5	87.5	.033
35	90.5	86.5	.023
40	93.5	83.5	.056
45	83	74	.057
50	80	67.5	.085

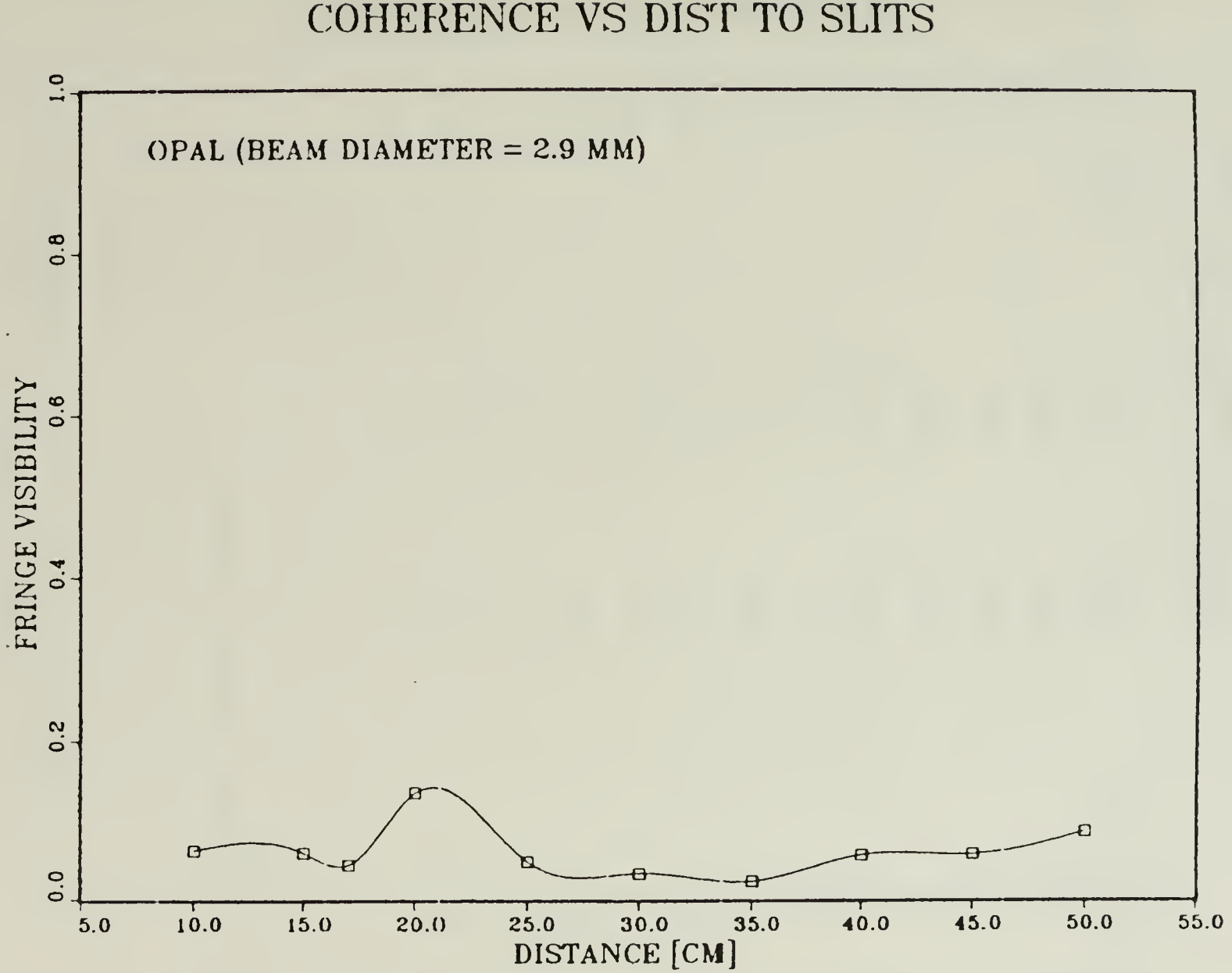

Figure 34. Plot of Coherence vs Distance for Opal (2.9 mm Beam)

TABLE VIII

FRINGE VISIBILITY RESULTS FOR OPAL GLASS IN A 3.6 MM BEAM

Distance (cm)	I_{max}	I_{min}	Fringe Visibility
15	107	90	.086
17.5	112	99	.062
18	112.5	102.5	.047
19	103.5	92.5	.056
20	112	99.5	.059
21	84	76.5	.047
25	108.5	98.5	.048
30	107.5	101.5	.029
35	109	91	.090
* 40	109	105	.019
45	111.5	98	.064
50	99	87	.065

* Interference pattern reduced 7%.

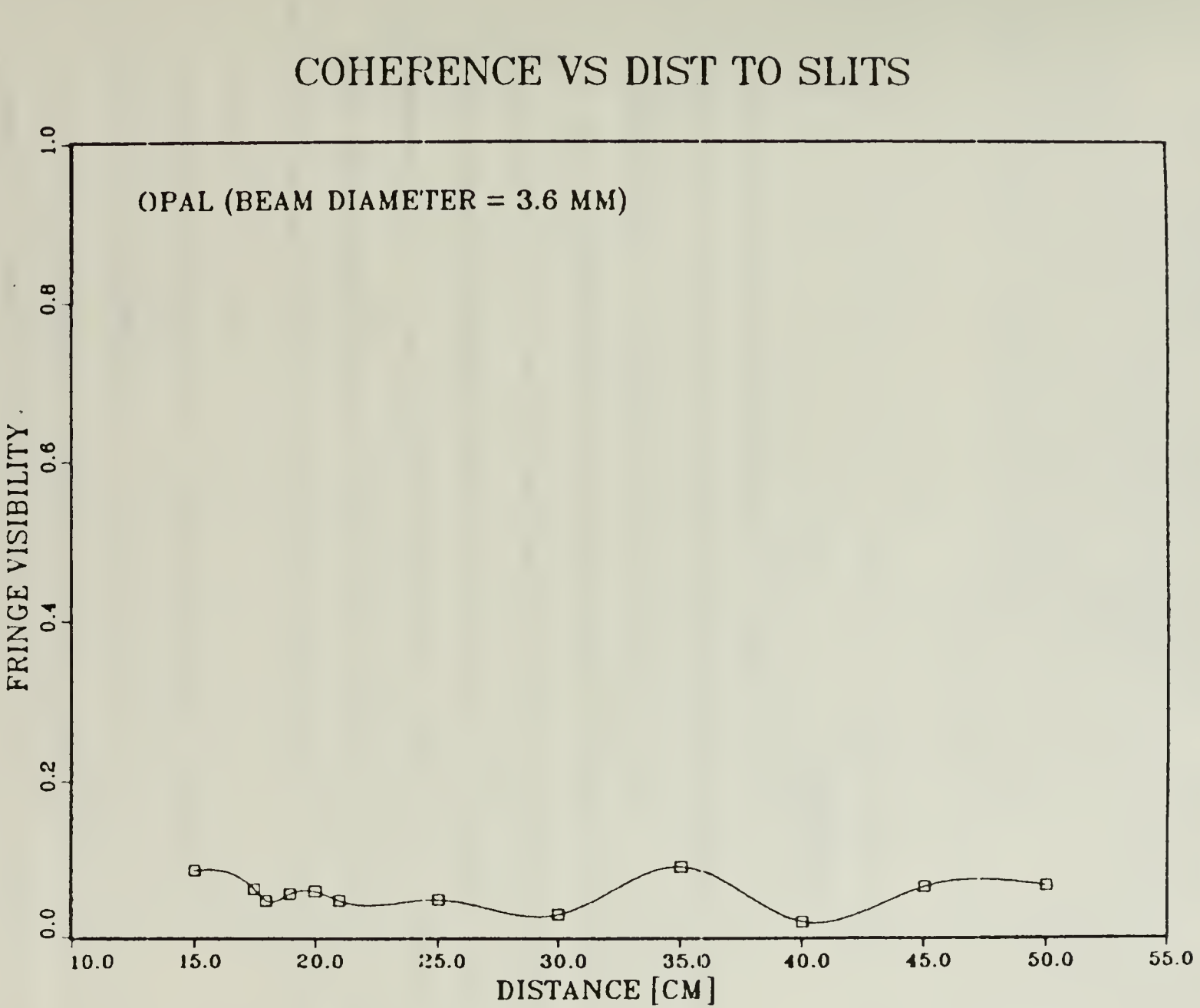

Figure 35. Plot of Coherence vs Distance for Opal (3.6 mm Beam)

Figures 34 and 35 show that the "position of incoherence" is no longer restricted to a single point when the beam diameter is increased. For a 2.9 mm beam the region of maximum coherence degradation appears to lie between 25 and 35 cm from the double slit. For a beam expanded to 3.6 mm, the average coherence degradation was 94% over a "region of incoherence" extending between 15 and 30 cm from the double slit.

E. ERROR ANALYSIS

1. Alignment

The experiment was very sensitive to alignment. A slight angular displacement between the double slits and the laser beam introduces a phase difference. A symmetrical interference pattern occurs only when segments of the primary wavefront arriving at the two slits are exactly in phase. The amount of angular displacement was reduced by utilizing the method of retro-reflection to obtain symmetry. That is, the reflected beam from the glass enclosing the double slits was adjusted with the incident beam so as to be collinear.

In order to maintain equal illumination on both slits the diffusive material must be aligned normal to the incident laser beam. If the diffusive medium is not perpendicular to the beam, the maximum intensity of the diffused beam will be displaced from the center of the

double slits due to refraction. Again, retro-reflection was used.

2. Effect of Finite Slit Width of the Photomultiplier Aperture

The photomultiplier integrates the incoming signal over the width of the slit. Ideally, for an infinitely narrow aperture slit, the fringe minima for a coherent source will touch the zero baseline. However, a finite slit width effectively integrates unwanted sections on either side of the minima of the incoming signal. Therefore, a "true" minima cannot be attained in the interference pattern. Figures 36 through 38 show the interference patterns without a diffusive medium for a pinhole aperture, a narrow slit aperture (.24 mm), and a wide slit aperture (1 mm), respectively. The width of the narrow slit approximately equals the diameter of the pinhole, therefore the coherence calculations are similar for the pinhole and narrow slit. The maximum coherence value measurable with the narrow aperture is $|\gamma_{12}(\tau)| = .94$--the effect of the aperture slit width is less than or equal to 6%. The maximum attainable coherence value for the wide slit aperture is $|\Gamma_{12}(\tau)| = .73$--this results in a false coherence degradation of as much as 27%! Therefore, the aperture size is an important consideration and the dimensions should be made as small as experimentally possible.

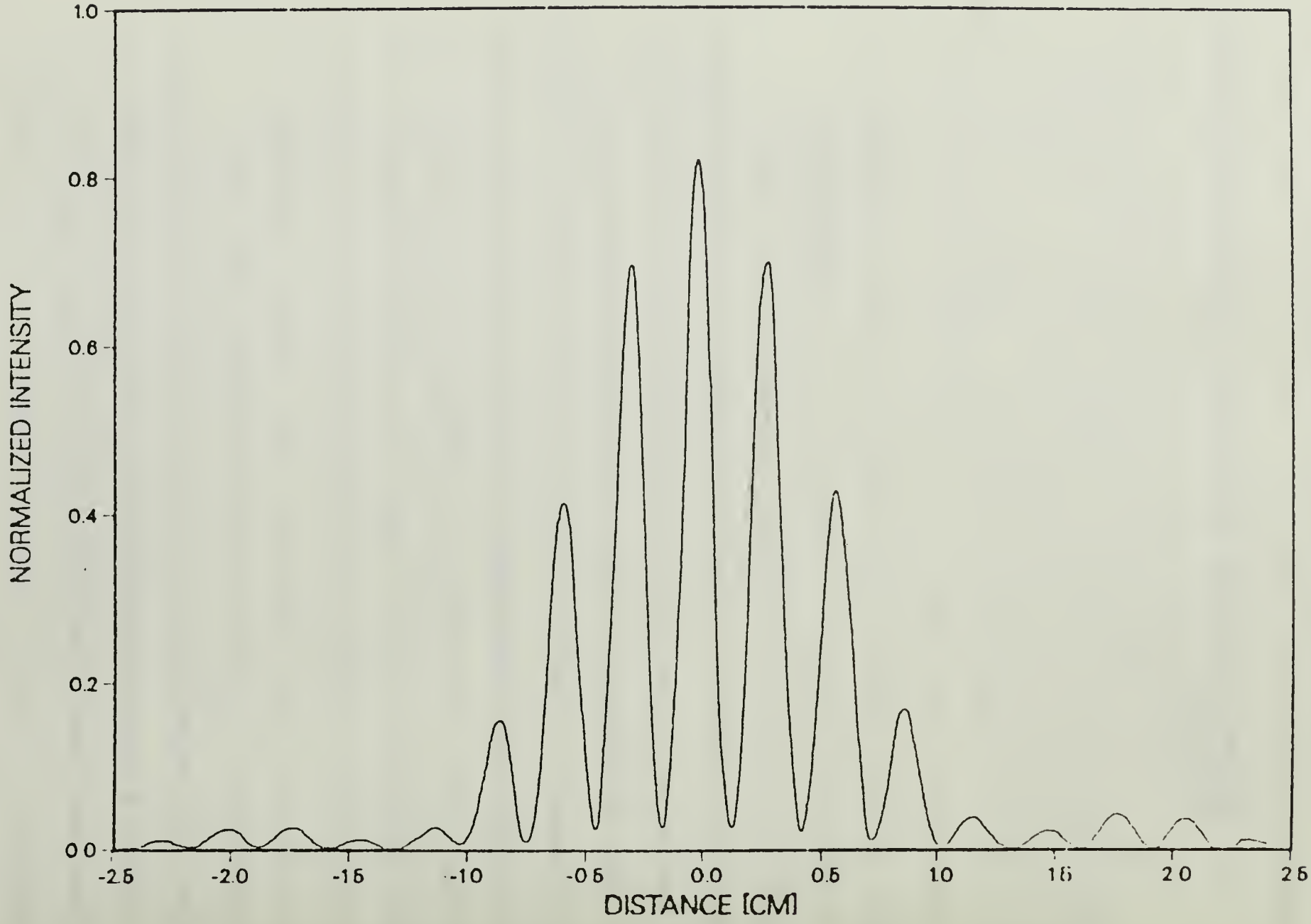

Figure 36. Interference Pattern Using Pinhole Aperture on PM Tube

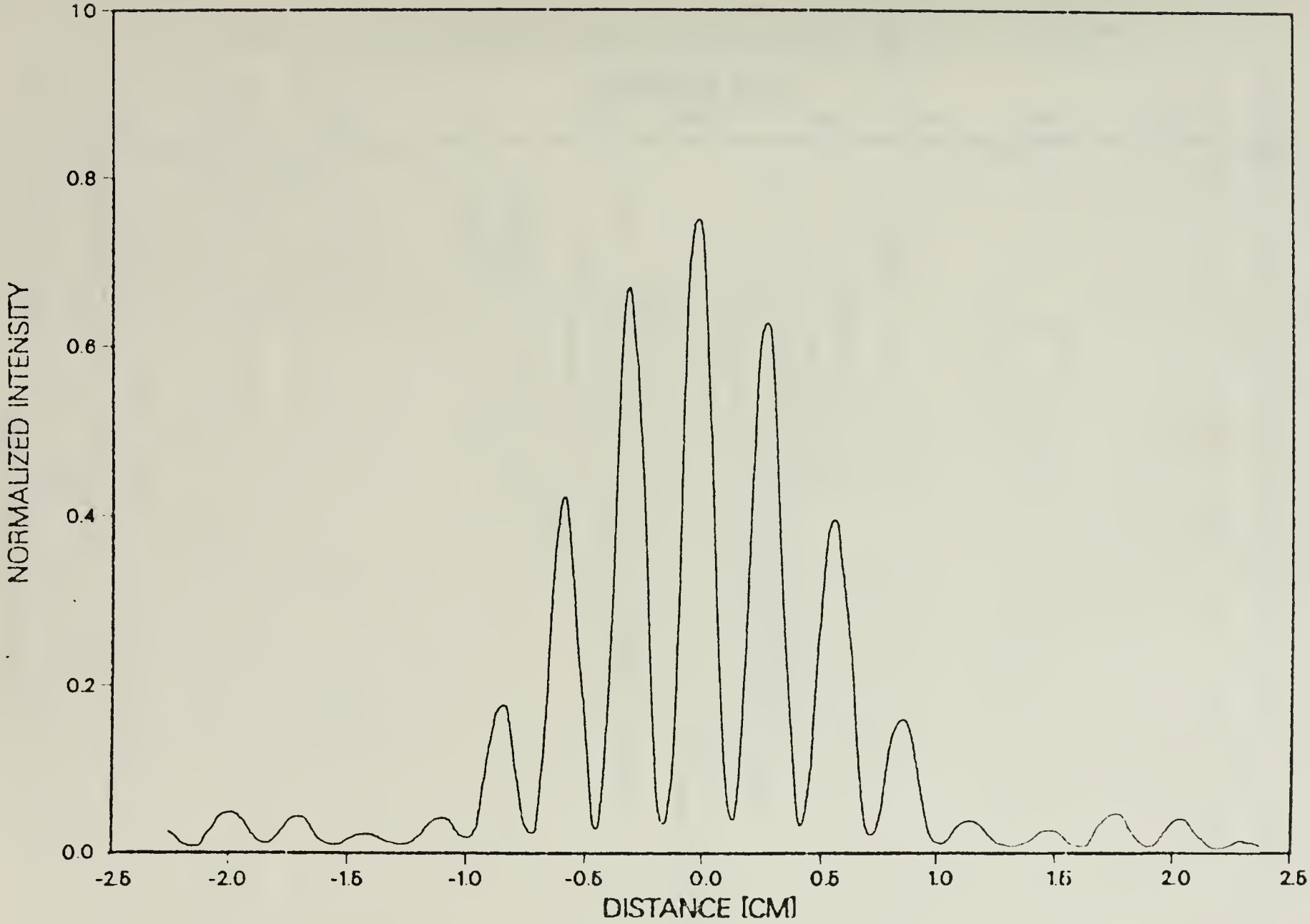

Figure 37. Interference Pattern Using Narrow Slit Aperture on PM Tube

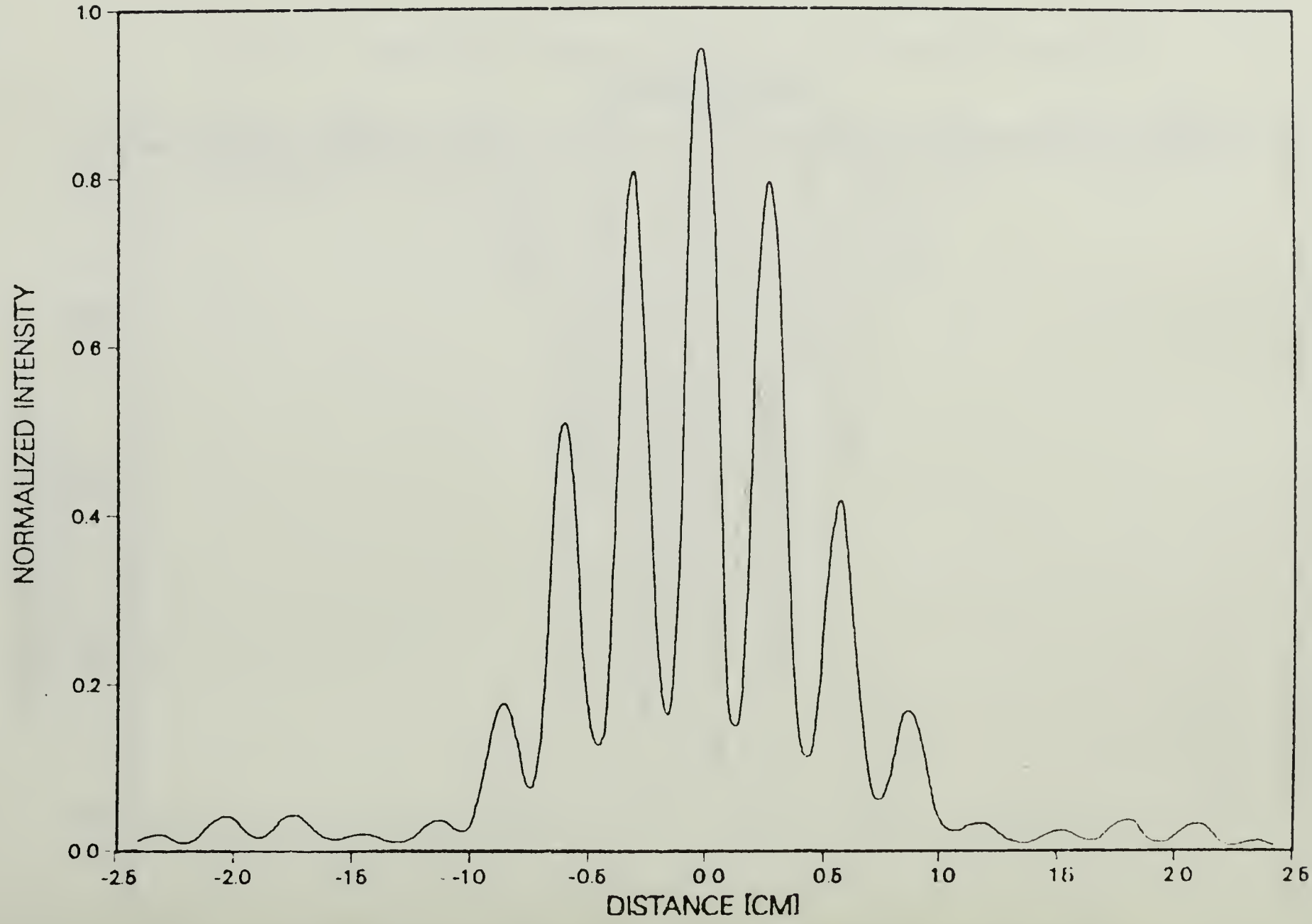

Figure 38. Interference Pattern Using Wide Slit Aperture on PM Tube

The effect various slit widths have on coherence measurements can be determined analytically. Integrating the incoming signal of the form, $f(x) = \sin x$, over an aperture slit width of B-A gives,

$$F(B-A) = \int_A^B f(x)dx = -(\cos B - \cos A) \quad . \qquad (17)$$

Normalizing and using a half-angle trigonometric identity,

$$\frac{F(B-A)}{B-A} = \frac{2 \sin \frac{1}{2}(B+A) \sin \frac{1}{2}(B-A)}{B-A} \quad . \qquad (18)$$

Choosing $(B+A)/2 = \pi/2$, eqn. 18 becomes,

$$\frac{F(B-A)}{B-A} = \frac{2 \sin \frac{1}{2}(B-A)}{B-A} \quad . \qquad (19)$$

Equation 19 is the modulation transfer function for a slit of width B-A. The periodicity of the interference fringes is 2.51 mm/cycle. Therefore, the .24 mm slit corresponds to .096 cycles or .6 radians. Substituting B-A = .6 radians into eqn. 19 gives $F(B-A)/(B-A) = .985$. Therefore, 1.5% of the original 6% coherence degradation is due to finite slit width and the remaining 4.5% is due to other factors.

Similarly, for the 1 mm slit, F(B-A)/(B-A) = .758. Therefore, of the original 27% coherence degradation, 24% is due to the finite slit width and 3% is due to factors such as scattered light.

Figure 39 shows a plot of the coherence for opal glass for fringe visibility calculations computed using the flat baselines compared to the coherence calculations computed using baselines corrected for slit width and scattered light. Figure 40 shows an interference pattern with the corrected baseline indicated with a dotted line. Figure 39 shows that the degree of coherence is not affected significantly by the effect of the narrow slit aperture and scattered light.

3. Scattered Light

In addition to the finite slit width, scattered light produces additional errors in the coherence measurements. Scattered light collected by the photomultiplier as well as internal reflections in the far field lens and the interference filter are error sources. In order to estimate the magnitude of the errors, the degree of coherence was measured before and after utilizing the lens and filter in the experiment. The lens-filter combination reduced the coherence from $|\gamma_{12}(\tau)| = .97$ to $|\gamma_{12}(\tau)| = .94$; therefore, it appears that the lens and filter account for approximately 3% of the coherence degradation.

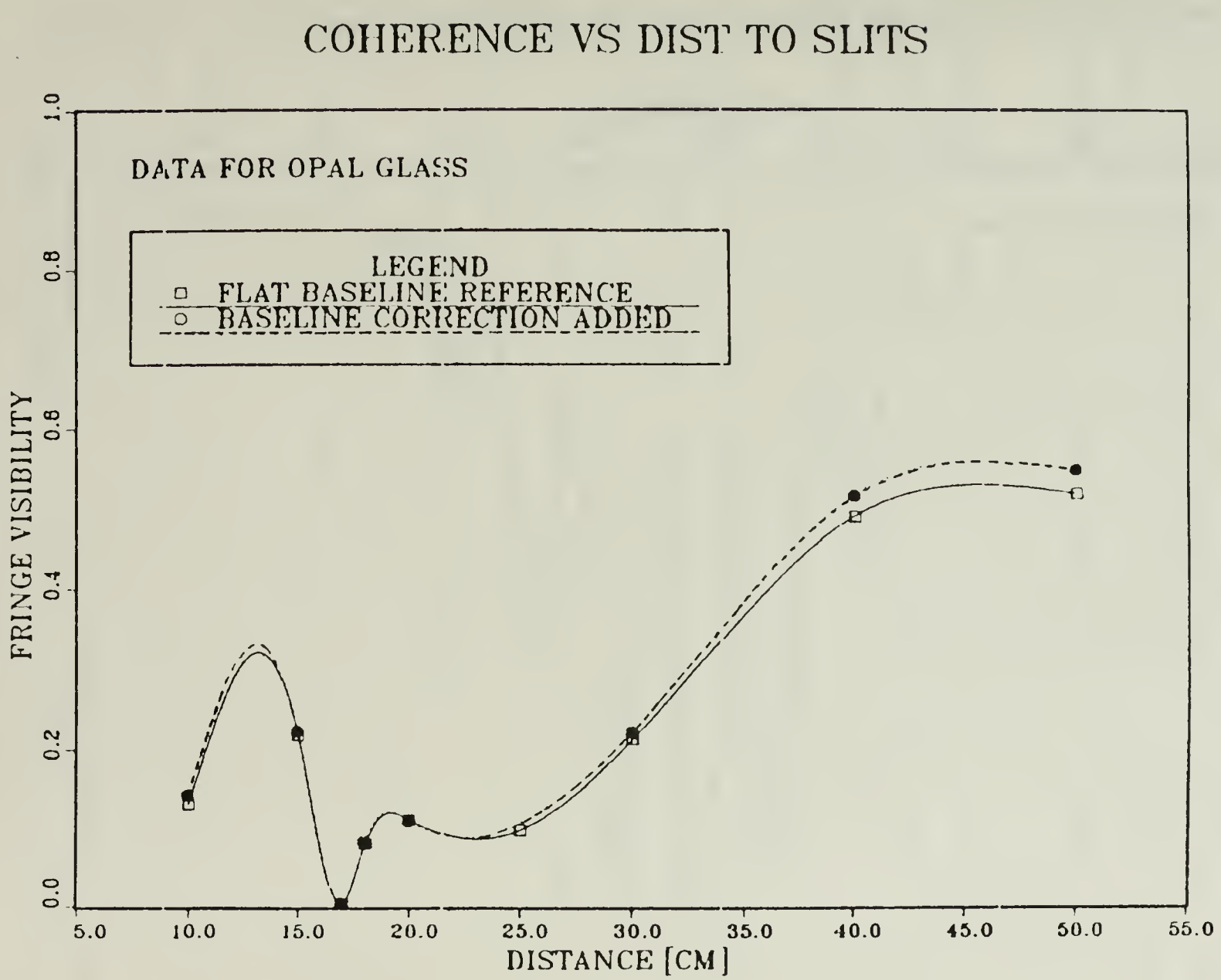

Figure 39. Plot Showing Effect of Finite Slit Width and Scattering on Coherence Measurements

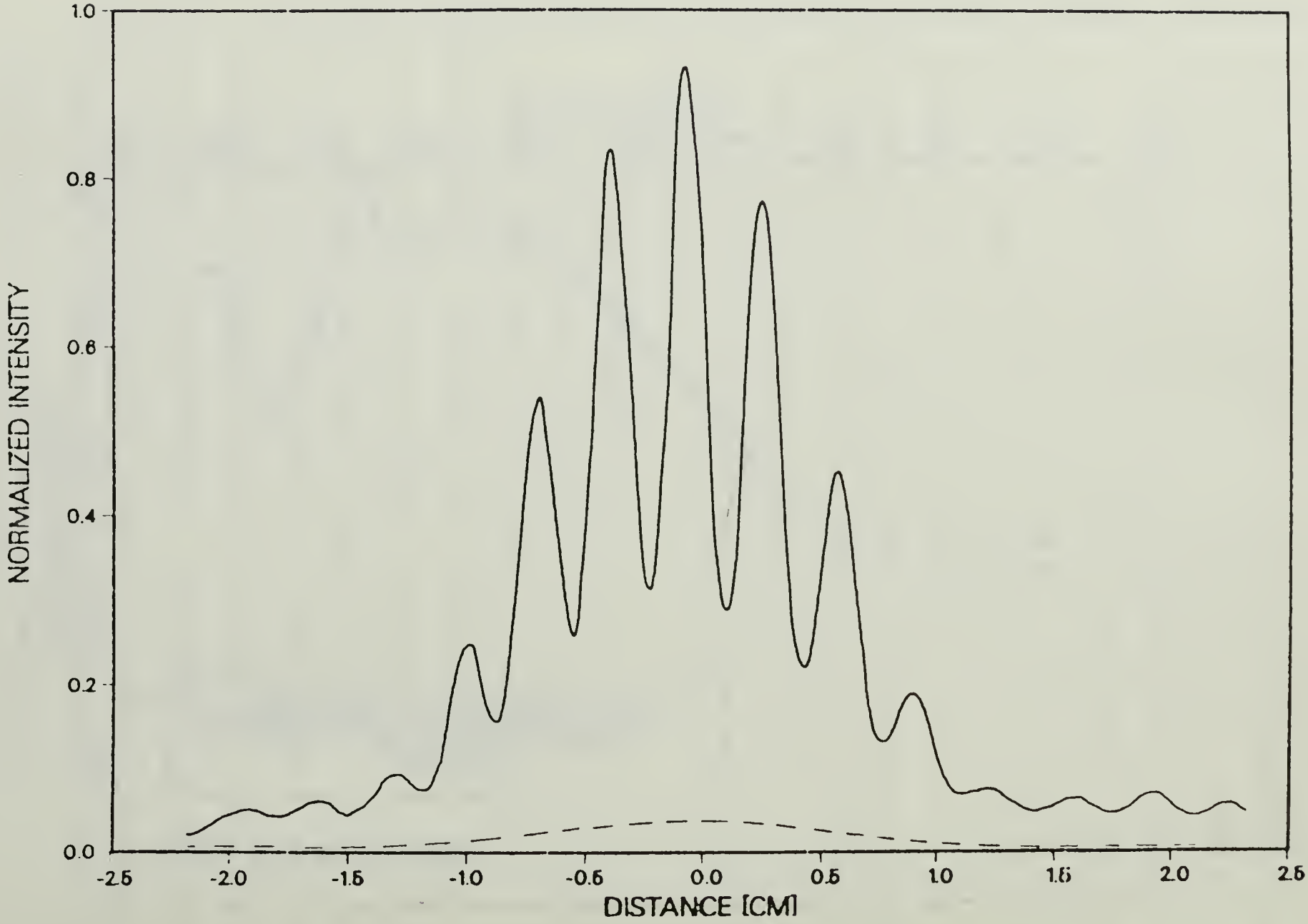

Figure 40. Interference Pattern with Baseline Corrected for Finite Slit Width and Scattering

The double slit, itself, introduces stray light into the experiment. If the slit material is not 100% opaque to the incident laser beam, a small portion of the beam will pass directly through the region between the slits. The glass casing for the double slit also introduces multiple internal reflections that contribute to the scattered light.

The lenses used to expand the beam in experiment #3 resulted in an additional 2% reduction of coherence. The maximum degree of coherence attainable with the 2.9 mm beam was $|\gamma_{12}(\tau)| = .92$.

Extraneous light sources, such as equipment pilot lights and the laser glow discharge, were a major source of error. These sources were shielded from the photo-multiplier with the use of tape and cloth. The cloth enclosure proved to be an effective method for preventing the scattered light from reaching the detector.

4. Fringe Visibility Measurements

A slight phase difference can be detected if the fringes in the interference pattern do not have the same height on both sides of the central maximum. Perfect symmetry was an ideal and rare occurrence. The assymetry of the pattern introduces errors in measuring the maximum and minimum intensities for calculating the fringe visibility, and hence, the coherence. The central fringe maximum does not always coincide with the diffraction maximum.

Therefore, the value of the diffraction maximum was determined and equated to I_{max} in order to maintain consistency in the measurements. The value for I_{min} was found by averaging the minimum values on both sides of the central fringe. A graph overlay (10 x 10 squares per half inch) provided the means to measure the maximum and minimum intensities. The readings were made to the nearest .025 inch (one half square) with an accuracy of $\pm$0.01 inches. This corresponds to a 1.4 percent error in the coherence calculations due to intensity measurements.

5. Double Slit Measurements

Using a traveling microscope and averaging a series of measurements, the slit separation, a, was .209 $\pm$ .002 mm, and the slit width, b, was .060 $\pm$ .002 mm.

The parameters a and b can also be determined analytically from the interference pattern. The spacing of the fringes is,

$$\Delta Y = \frac{\lambda S}{a} , \qquad (20)$$

where λ = 488 nm, S = 1.033 m, and ΔY = 2.51 mm. Therefore, the calculated slit separation is .201 mm, in good agreement with the .209 mm measured value. The location of the first diffraction zero is obtained from the relationship,

$$\sin \theta = \frac{\lambda}{b} , \qquad (21)$$

where for small angles, $\sin \theta = \tan \theta = d/S$, and d equals the distance from the principal maximum to the first diffraction zero. Using d = 11.5 mm, the calculated slit width, b, equals .044 mm compared to the measured .06 mm.

Comparing the calculations obtained from the geometry of the interference pattern with the measured values results in an error of 3.8% for a, and 26.6% for b. The large error in calculating the slit width is attributed to the Gaussian intensity of the beam illuminating the double slit. The intensity is not uniform across the slit width. By increasing the beam diameter the Gaussian intensity pattern begins to approach the shape of the "top hat" function over the width of the slit. Figure 41 compares the single slit diffraction patterns for the 1.5 mm beam and the 3.6 mm beam. For a 3.6 mm beam, the diffraction minima moves closer to the central maximum. The "new" slit width is .052 mm, reducing the error to 13.3%. Therefore, the beam diameter must be large compared to the slit width in order to achieve agreement between the experimental single slit diffraction pattern and the theoretical, uniformly-illuminated, single slit diffraction pattern.

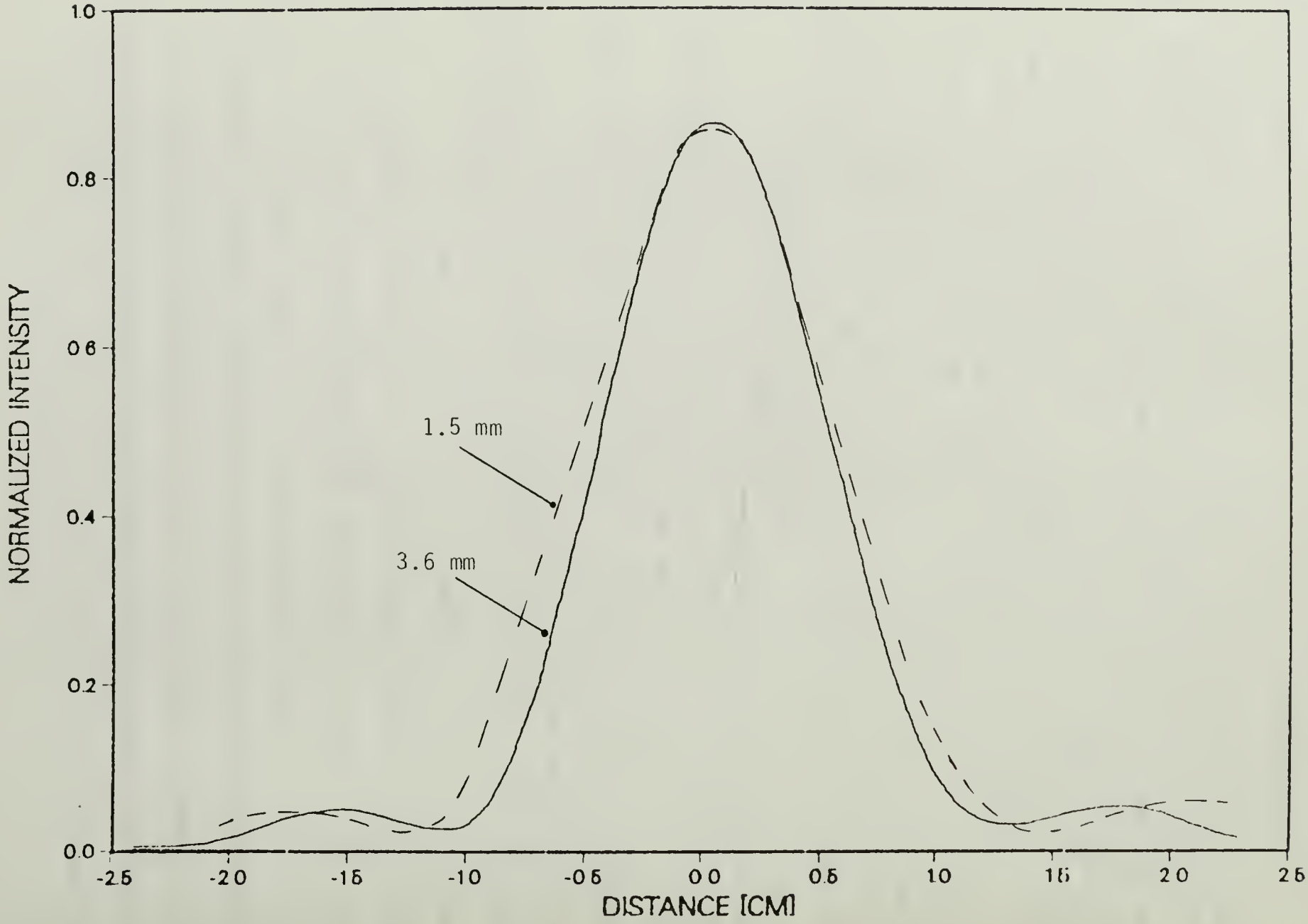

Figure 41. Slit Slit Diffraction Patterns for Beams with Different Diameters

V. CONCLUSION

From the results of this experiment it can be concluded that the spatial coherence of a laser source can be degraded by as much as 99.5% by placing an opal diffuser at a specific position (17 cm) between the laser and the double slit. Increasing the beam diameter incident on a diffuser eliminates the sharp minimum in the coherence vs. distance curve and reduces the spatial coherence over a broad range of laser to diffuser distances. For a beam expanded to 3.6 mm, the average coherence degradation was 94.7% over a "region of incoherence" extending over a 10 cm interval.

Future research is necessary to determine the effect different experimental geometries have on the degree of spatial coherence and to justify the behavior of the incoherence location analytically. In particular, the van Cittert-Zernike theorem should be applied to the calculation of the degree of spatial coherence. Suggested modifications of the experiment involve changing the distance between the laser and double slit, utilizing various sizes and widths for diffusers, and expanding the laser beam to larger diameters. Future investigations should include use of a digital frequency analyzer to sample and process data on a near real time basis.

APPENDIX A

PROOF THAT F.V. = $|\gamma_{12}(\tau)|$

To show that the fringe visibility at point P of Figure 1 is equal to the degree of coherence of the electric field between points S_1 and S_2, the superposition of the analytic signals from the two points must be determined. The analytic signal is,

$$V = K_1 V(S_1, t'-t_1) + K_2 V(S_2, t'-t_2) \quad , \tag{A1}$$

where $t_1 = \frac{L_1}{c}$ and $t_2 = \frac{L_2}{c}$. According to Beran and Parrent [Ref. 7] the K_1 and K_2 factors are independent of time, inversely proportional to L_1 and L_2, and dependent on the size of the slits and the angle to P. The intensity P, from eqn. 1, is given by,

$$I = \langle VV^* \rangle = I_1(t+\tau) + I_2(t) + 2K_1K_2^* \mathrm{Re}\,[\langle V(S_1,t+\tau)V^*(S_2,t)\rangle] \tag{A2}$$

where $t = t' - t_2$ and $\tau = t_2 - t_1$. I_1 and I_2 are the intensities at point P due to the emission from point S_1 and point S_2 alone. The term inside the brackets is the mutual coherence function as defined in eqn. 5. Therefore, eqn. A2 becomes,

$$I = I_1 + I_2 + 2K_1K_2^* \text{ Re } [\Gamma_{12}(\tau)] \quad . \tag{A3}$$

When S_1 and S_2 are made to coincide, the normalized mutual coherence functions from eqn. 7 become,

$$\Gamma_{11}(0) = \langle V_1(t)\ V_1^*(t) \rangle$$

and

$$\Gamma_{22}(0) = \langle V_2(t)\ V_2^*(t) \rangle \quad . \tag{A4}$$

Using equation 6 and noting that,

$$K_1K_2^* [\Gamma_{11}(0)\ \Gamma_{22}(0)]^{1/2} = [|K_1|^2\ \Gamma_{11}(0) |K_2|^2\ \Gamma_{22}(0)]^{1/2}, \tag{A5}$$

eqn. A3 becomes,

$$I = I_1 + I_2 + 2[I_1\ I_2]^{1/2} \text{ Re}[\gamma_{12}(\tau)] \quad . \tag{A6}$$

If Zernike's "best circumstances" are used from Chapter III.D ($I_1 = I_2 = I$ and the path differences are small), and if the complex degree of coherence is written in the form,

$$\gamma_{12}(\tau) = |\gamma_{12}(\tau)| \exp[i\phi_{12}(\tau)] \quad , \tag{A7}$$

eqn. A6 can be written as,

$$I = 2I[1 + |\gamma_{12}(\tau)| \cos \phi_{12}(\tau)] \quad . \tag{A8}$$

From eqn. 10, the fringe visibility becomes,

$$F.V. = \frac{2I[(1 + |\gamma_{12}(\tau)|) - (1 - |\gamma_{12}(\tau)|)]}{2I[(1 + |\gamma_{12}(\tau)|) + (1 - |\gamma_{12}(\tau)|)]} \quad . \tag{A9}$$

Therefore,

$$F.V. = |\gamma_{12}(\tau)| \quad . \tag{A10}$$

LIST OF REFERENCES

1. Svelto, O., Principles of Lasers, 2nd edition, p. 270, Plenum Press, 1982.

2. Wolf. E., "Coherence and Radiometry," Optical Society of America, v. 68, p. 8, January 1978.

3. Hecht, E. and Zajac, A., Optics, p. 426, Addison-Wesley, 1979.

4. Beran, M.J. and Parrent, G.B., Theory of Partial Coherence, p. 4, Prentice-Hall, 1964.

5. Zernike, F., "The Concept of Degree of Coherence and Its Applications to Optical Problems," Selected Papers on Coherence and Fluctuations of Light, v. 1 1950-1960, p. 101, Dover, 1970.

6. Born, M. and Wolf., Principles of Optics, p. 509, Pergamon Press, 1975.

7. Beran, M.J. and Parrent, G.B., Theory of Partial Coherence, p. 10, Prentice-Hall, 1964.

INITIAL DISTRIBUTION LIST

		No. Copies
1.	Defense Technical Information Center Cameron Station Alexandria, Virginia 22314	2
2.	Library, Code 0142 Naval Postgraduate School Monterey, California 93943	2
3.	G. E. Schacher, Chairman, Code 61Sq Department of Physics Naval Postgraduate School Monterey, California 93943	2
4.	Professor D. L. Walters, Code 61We Department of Physics Naval Postgraduate School Monterey, California 93943	2
5.	Professor E. A. Milne, Code 61Mn Department of Physics Naval Postgraduate School Monterey, California 93943	2
6.	LT J. S. Peterson 2976 Curlew Street San Diego, California 92103	2

210533

Thesis
P4143 Peterson
c.1 A spatially incoherent and temporally coherent source.